UNIVERSITÀ DEGLI STUDI DI PALERMO

Dottorato in Ingegneria dell'Innovazione Tecnologica - Ciclo XXX
Dipartimento dell'Innovazione Industriale e Digitale
Chimica Fisica Applicata

DISTRETTO TECNOLOGICO
SICILIA MICRO E NANO SISTEMI
S.C.A.R.L.

NANOSTRUCTURED ELECTRODES FOR HYDROGEN PRODUCTION IN ALKALINE ELECTROLYZER

Ph. D. Candidate
FABRIZIO GANCI

Ph. D. Committee Chief
Prof. CHELLA ANTONINO

Supervisor
Prof. CARMELO SUNSERI

Co-Supervisor
Prof. ROSALINDA INGUANTA
Dr. SALVATORE LOMBARDO

CICLO XXX
Anno Accademico 2018

Table of Contents

Acknowledgements

First, I want to thank the Distretto Tecnologico Sicilia Micro e Nano Sistemi S.c.a.r.l. in Catania for funding my PhD position, giving me the opportunity to grow professionally and humanely beyond my expectations.

I wish to thank the scientists at NREL (National Renewable Energy Laboratory, Denver, Colorado) for welcoming me to their laboratory facilities. In particular, I want to thank Bryan Pivovar, Guido Bender, and Huyen Dinh for their patience and for their valuable teachings during my time in the United States.

Last but not least, I want to thank the Laboratory of Applied Physics Chemistry of the University of Palermo, which welcomed me three years ago despite being a "poor" energy engineer. In particular, a special thanks to my tutor, Prof. Carmelo Sunseri, and to my co-tutor, Prof. Rosalinda Inguanta. An affectionate thought also goes to Prof. Salvatore Piazza, with whom I spent one of the best experiences of these 3 years at the International Society of Electrochemistry meeting in The Hague.

Research Results Dissemination

Publications on International Journals:

1. Ganci F., Inguanta R., Piazza S., Sunseri C., Lombardo S. (2017) *Fabrication and Characterization of Nanostructured Ni and Pd Electrodes for Hydrogen Evolution Reaction (HER) in Water Alkaline Electrolyzer*, CET vol. 57, 1591-1596.
2. Sunseri C., Cocchiara C., Ganci F., Moncada, A., Oliveri R. L., Patella B., Piazza S., Inguanta, R (2016) *Nanostructured Electrochemical Devices For Sensing, Energy Conversion And Storage*, CET vol. 47, 43-48.
3. Caruso M., Castiglia V., Miceli, R., Nevoloso C., Romano P., Schettino G., Viola, F., Insinga M.G., Moncada A., Oliveri R.L., Ganci F., Sunseri C., Piazza S., Inguanta, R. (2017) *Nanostructured lead acid battery for electric vehicles applications* 2017, International Conference of Electrical and Electronic Technologies for Automotive, Article number 7993216.
4. Insinga M. G., Moncada A., Oliveri R. L., Ganci F., Piazza S., Sunseri C., Inguanta, R. (2017) *Nanostructured Pb Electrode for Innovative Lead-acid Battery*, CET vol. 60, 49-54.
5. Ganci F., Lombardo S., Sunseri C., Inguanta R. (2018) *Nanostructured electrodes for hydrogen production in alkaline electrolyzer*, Renewable Energy, Elsevier, https://doi.org/10.1016/j.renene.2018.02.033

Memories presented at International Congresses:

- Ganci F., Piazza S., Sunseri C., Lombardo S., and Inguanta R. (2017) *Ni and Ni-Pd nanostructured electrodes for water-alkaline electrolysers*, HYPOTHESIS XII, Siracusa, 28th - 30th June 2017.
- Ganci F., Inguanta R., Piazza S., Sunseri C., Lombardo S. (2017) *Fabrication and Characterization of Nanostructured Ni and Pd Electrodes for Hydrogen Evolution Reaction (HER) in Water Alkaline Electrolyzer,* 13th International Conference on Chemical and Process Engineering, Milan, 28th – 31st May 2017.
- Ganci F., Inguanta R., Piazza S., Sunseri C., Lombardo S. (2016) *Electrodeposition And Caracterization Of Nanostructured Ni And Ni-IrO2*; International Society of Electrochemistry, The Hague, Netherlands, 22nd - 26th August 2016.
- Ganci F., Inguanta R., Piazza S., Sunseri C., Lombardo S. (2016) *Fabrication Of Nanostructured Ni And Ni-Pd Electrodes For Water-Alkaline Electrolyzer*; International Society of Electrochemistry, The Hague, Netherlands, 22nd - 26th August 2016
- Inguanta R., Cocchiara C., Ganci F., Moncada A., Patella B., Piazza S., Sunseri C., Lombardo S. (2015) *Nanostructured materials for sensing, energy conversion and storage*; X INSTM CONFERENCE, Favignana (TP), 28th June – 1st July 2015.

Patent (submitted):

Inguanta R., Ganci F., Insinga M. G., Sunseri C., *High Specific Energy Alkaline Electrolyzer with Nanostructured Electrodes*,.

Nomenclature

Acronyms

1D	One-Dimensional
AWE	Alkaline Water Electrolysis
CV	Cyclic Voltammetry
EDS	Energy Disperse Spectroscopy
HER	Hydrogen Evolution Reaction
HHV	Higher Heat Value
KOH	Potassium Hydroxide
LHV	Lower Heat Value
MEA	Membrane Electrode Assembly
NWs	Nanowires
PEM	Polymer Electrolyte Membrane or Proton Exchange Membrane
RHE	Reversible Hydrogen Electrode
SCE	Saturated Calomel Electrode
SEM	Scanning Electron Microscope
SOEC	Solid Oxide Electrolysis Cell
STP	Standard Temperature and Pressure: 298.15 °K and 1 atm
WE	Working Electrode
XRD	X-Ray Diffraction
YSZ	Yttria Stabilized Zirconia

1. Introduction

The current global energy system is currently based on fossil fuels. They are the primary source of carbon dioxide, a gas recognized as the main responsible for the greenhouse effect and consequent global warming. In the future, the problem will be enhanced owing to the increase of the world population from the current 7.4 to over 9 billion estimated for 2040, increasing the total energy demand by 30% [1]. A possible solution could come from the use of renewable sources, which already occupy a portion of primary energy production. However, the energy produced by some of these sources, such as solar or wind, has an aleatory character, which depends for example on the day-night cycle but also on the season of the year. This problem is stressing the importance of storing energy when overcomes the demand, in order to supply it when demand is higher [2]. A Boston Consulting Group analysis [3] estimates that between 2015 and 2030 the volume of the global energy storage market will grow from 6 to 26 billion euro. Among the various storage systems, hydrogen will undergo the greatest growth and in 2030 will cover 19% of the global market. The use of hydrogen as an energy vector is an idea that has been present for decades [4]. The coupling of a renewable energy source to an electrochemical cell is an example of effective storage system for renewable plants that could, in the future, replace the use of fossil fuels, thus opening the way to the so-called Hydrogen Economy [5].

The main obstacle to using hydrogen as an energy carrier is its availability. CH_4 reforming is currently the most diffuse production process, because the hydrogen final cost is very low in comparison with

other methods [6]. Among these, the electrochemical water splitting is highly attractive because it is environmental friendly, very flexible, and easy to be conducted. Unfortunately, the process is very expensive because electrical charge is the driving reagent. In particular, 53.6 Ah under a thermodynamic potential of 1.23 V are necessary for producing one mole of hydrogen. Really, the thermodynamic potential to be considered is 1.48 V owing to the heat supply associated with entropy increase accompanying the water splitting reaction. Therefore, the theoretical energy consumption is of 39.664 Wh per gram of hydrogen. The real value is higher owing to the electrochemical process irreversibility. It is precisely for that reason that the present research has been focused on the study of the electrochemical cell with specific attention toward the electrocatalysis issues in order to separate its contribute from that one due to the cell design.

At this aim, the use of nanostructured electrodes was investigated to decrease the reaction overvoltage through a significant increase of the electrode surface. Nickel-based nanostructured electrodes were fabricated and tested in alkaline solutions at room temperature. The attention was devoted to alkaline solutions, because the alternative acidic baths require platinum-based electrodes, which, of course, are very expensive. Therefore, a less noble material has been chosen in the light of a strong cost reduction. The temperature was maintained at ambient values, because the interest was in the investigating the electrode performance in the less favorable conditions. In this scenario, the cell design was not optimized because it was thought of primary importance to identify first of all, the major contributes to the overvoltage.

Consequently, an electrochemical cell was assembled only for testing the electrodes at current densities of 0.5 Acm^{-2} that is the lower value of technological interest. Ni-based, and Pd electrodes with different morphologies were tested, in order to enhance the role of the nanostructures. From this point of view, Ni nanostructured electrodes revealed better performances than all other ones, Pd included. Despite Pd is a well-known good catalyst for reactions involving hydrogen, it is limited by the high capacity of adsorbing inversion determining a fast decay of its performance as an electrocatalyst.

The research activity was planned in collaboration with the Institute of Microelectronics and Microsystems (IMM) of the CNR in Catania, for the study of a concentration photovoltaic system to power the electrolyzer. Unfortunately, this issue has not been sufficiently scrutinized, because the issues concerning the electrochemical process required long times of investigation. On the other hand, the hydrogen production through PEM-type electrochemical cell has been investigated during a stay in NREL Labs at Denver-Colorado.

As for the alkaline cells, the fabrication of nanostructured electrodes through template electrosynthesis was deeply investigated looking for correlating nature and morphology of the electrode with its electrochemical performances. Different characterization techniques were used such as Energy Dispersion Spectroscopy, X-Ray Diffraction, Scanning Electron Microscopy, and Cyclic Voltammetry conducted in 30% w/w KOH aqueous solution, as electrochemical tests. Also long time electrode stability under hydrogen evolution was tested.

References

[1] World Energy Outlook 2017 – International Energy Agency http://www.iea.org/weo/

[2] Shiroudi A., Taklimi S. R. H., Jafari N. (2012) *Case study: Technical assessment of the efficiency optimization in direct connected PV-Electrolysis system at Taleghan-Iran*, Journal of Renewable and Sustainable Energy, 4.

[3] LBS GES 2014 - Keynote 3 - Holger Rubel, BCG. http://www.slideshare.net/globalenergysummit/lbs-ges-2014-keynote-3-holger-rubel-bcg

[4] Ulleberg O. (2003) *Modeling of advanced alkaline electrolyzers: a system simulation approach*, International Journal of Hydrogen Energy, 28, 21–33.

[5] Momirlan M., Veziroglu T. N. (2002) *Current status of hydrogen energy*, Renewable and Sustainable Energy Reviews, 6, 141–179.

[6] Marcelo D., Dell'Era A. (2008) *Economical electrolyser solution*, International Journal of Hydrogen Energy, Elsevier, 33, 3041–3044.

2. Hydrogen Economy

Hydrogen is the first element of the periodic table and the smallest element in the Universe. It is also the most abundant, about 75 wt.% and 90 vol.% of all matter. On earth, it is almost always bond to other elements, such as oxygen (water) and carbon (hydrocarbons), and it is almost impossible found it in molecular form.

At STP, hydrogen is a colorless, odorless, tasteless, non-toxic, and highly combustible diatomic gas. It has many important properties [1]; its fusion and boiling points are 14.02 K and 20.27 K, respectively. Molecular hydrogen has a wide concentration range of flammability (4-75% by volume) and explosiveness (4-74% by volume) with air, and its autoignition temperature is 500 °C. It is the fuel with the highest heat values (141.80 MJ/kg HHV, 119.96 MJ/kg LHV), more than two times higher than all the other fuels, but it has a low volumetric energy density (2.1 kJ/m^3). This is due to the low density (0.0899 g/dm^3 at STP).

Hydrogen has many uses [2]; the most important are the production of ammonia and methanol, and oil refining (desulphurization and hydrocracking), which consume 95% of global hydrogen production (Fig. 2.1), taken as a whole. In the food industry, hydrogen is used for unsaturated vegetable oils hydrogenation. In metal and cement industries, it is used as reductive agent. In space and aeronautics application, it is consumed as rocket fuel in the liquid state.

However, in the next decades, the hydrogen role could become more relevant in the world's energy scenario. In fact, hydrogen is being considered the future energy carrier [3-6]. In addition to the already mentioned hydrogen properties, another important one is the hydrogen

combustion with oxygen that can produce energy and/or heat without carbon dioxide production.

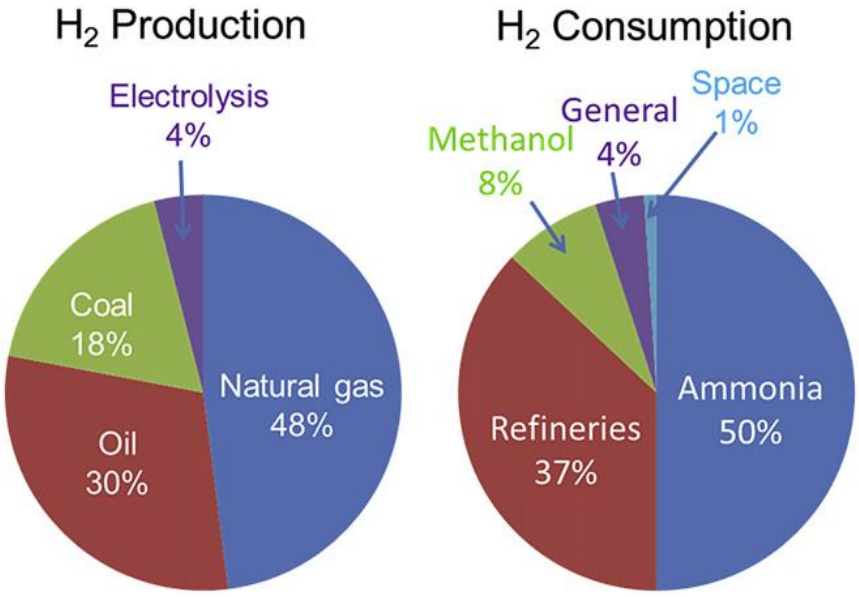

Figure 2.1 - World hydrogen production and consumption. [11].

Nowadays, one relevant hindrance to the hydrogen economy growth is the impossibility to found hydrogen in nature, unlike others fuel. Furthermore, hydrogen production is mostly carried out using fossil fuels. In addition to hydrogen, these production processes also produce carbon monoxide and dioxide, making them environmentally unsustainable [7-9]. However, they are cheaper in comparison with other greener processes, like electrolysis or photo-electrolysis.

The hydrogen production methods will be discussed in chapter 2.1. Storage and transport are other two important issues to be considered in hydrogen technology. They will be treated in chapter 2.2.

2.1. Hydrogen Production

The annual hydrogen production is estimated at about 50 million tons [10]. As evidenced in Fig. 2.1, hydrogen production is mostly carried out using fossil fuels; in particular, hydrogen production from natural gas steam reforming is 48% of the total, partial oxidation of oil 30%, coal gasification 18%. Another small part of hydrogen comes from electrolysis (4%), which gives the most pure gas, highly desired in the food industry. Electrical energy supplies electrochemical cell to split water in hydrogen and oxygen. This method will be discussed in chapter 3.

Table 2.1 – Production processes, raw materials, and energy sources [12].

	Processes	Raw Materials	Source of Energy
Electrochemical	Electrolysis	• Water	• Electricity from renewable energy sources (e.g., wind, geothermal, solar, hydro) • Electricity from nonrenewables (e.g., fossil fuels, nuclear)
Thermochemical	Reforming	• Natural gas • Hydrocarbons • + Water	• Combustion of natural gas/syngas • Concentrating solar thermal
	Gasification	• Coal • Carbonaceous materials • Biomass • + Water	• Combustion of coal/biomass/ carbonaceous materials/syngas • Concentrating solar thermal
	Decomposition	• Natural gas • Fossil fuel hydrocarbons • Biomethane • Biohydrocarbons	• Natural gas combustion • Concentrating solar thermal
	Thermolysis	• Water	• Concentrating solar thermal
	Thermochemical cycles	• Water	• Concentrating solar thermal • Nuclear heat
Photochemical	Photosynthesis	• Water	• Solar radiation, artificial light
	Photobiological	• Microbial (e.g., algae) • + Water	• Solar radiation

There are two substantial differences between electrolysis and fossil fuel-based methods. The production cost is smaller for the last

respect to electrolysis because of higher electrical energy cost in comparison to natural gas, oil or coal. On the other hand, electrolysis process is environmentally sustainable because it does not generate carbon monoxide and dioxide as co-product, and, in addition, hydrogen by electrolysis reaches a purity grade (99.99%) that is impossible to reach with other methods, unless to provide expensive purification processes, which may waste every economic advantage.

Hydrogen can be produced through electrochemical, thermochemical, and photochemical processes, according to Table 1. This classification is based on the kind of energy input. In electrochemical processes, the energy input is electrical energy that can be supply by renewable and nonrenewable sources. In thermochemical processes, the energy input is high-temperature heat that can be supplied by renewable and nonrenewable sources. In photochemical processes, the energy input is by the direct absorption of light photons.

Details of some production processes are given below.

2.1.1. Steam Reforming

Steam reforming was developed in Germany at the beginning of the 20th century, to produce hydrogen for ammonia synthesis, and was further developed in the1930s when natural gas and other hydrocarbon feedstocks such as naphtha became available on a large scale [13].

Steam reforming is the most used and the cheapest process to produce hydrogen. It uses thermal energy to separate hydrogen from the carbon components of hydrocarbons, usually natural gas, and involves the reaction of these fuels with steam on catalytic surfaces [14]. The first step of the reaction is the decomposition of the fuel into hydrogen and carbon

monoxide (Eq. 2.1), followed by the water-gas shift reaction of the carbon monoxide and water to carbon dioxide and hydrogen (Eq. 2.2)

$$CH_4 + H_2O \rightarrow CO + 3H_2 \qquad \Delta H^{\circ}_{298} = 206.3 \text{ kJ/mol} \quad (2.1)$$

$$CO + H_2O \rightarrow CO_2 + H_2 \qquad \Delta H^{\circ}_{298} = -41.1 \text{ kJ/mol} \quad (2.2)$$

Steam reforming reaction [1] is endothermic, hence some of the fuel must be burned and the heat transferred to the reformer via heat exchangers. The process is operated at high temperatures (up to 1000 °C) and moderate pressures (25–35 bar). Steam reforming is a catalytic process; the used catalyst is typically Ni- based supported on Al_2O_3 and $MgAl_2O_4$. The steam reforming efficiency is around 65-70% [15].

Steam reforming of light hydrocarbon is also a well-established industrial process. An example is methanol steam reforming. It can be conducted from renewable sources and the reforming reaction occurs at relatively low temperatures, ca. 240–260 °C [16]. The most common catalysts are based on copper, such as $Cu/ZnO/Al_2O_3$. Methanol steam reforming process can be described by the following chemical reactions:

$$CH_3OH + H_2O \rightarrow CO_2 + 3H_2 \qquad \Delta H^{\circ}_{298} = 49.7 \text{ kJ/mol} \quad (2.3)$$

$$CH_3OH \rightarrow CO + 2H_2 \qquad \Delta H^{\circ}_{298} = 90.7 \text{ kJ/mol} \quad (2.4)$$

$$CO + H_2O \rightarrow CO_2 + H_2 \qquad \Delta H^{\circ}_{298} = -41.1 \text{ kJ/mol} \quad (2.5)$$

2.1.2. Partial Oxidation

Partial oxidation is an alternative to steam reforming and is generally employed with higher hydrocarbons or if pure oxygen is available [17]. It is an exothermic reaction that converts fuel in syngas (CO and H_2) using a substoichiometric amount of oxygen. Partial

oxidation process can occur either with or without catalyst. The non-catalytic process operates at temperatures in the range of 1200-1500 °C and pressure above 3 MPa. With catalyst, partial oxidation can be carried out at lower temperature (around 1000 °C). As compared to steam reforming, catalytic partial oxidation has the advantage of short start-up time because the reaction is exothermic, but for pure hydrogen production it is less efficient and more expensive [12, 18].

A general equation for partial oxidation is shown below.

$$C_xH_yO_z + \frac{(x-z)}{2}O_2 \rightarrow xCO + \frac{y}{2}H_2 \qquad \Delta H^{\circ}_{298} < 0 \text{ kJ/mol} \qquad (2.6)$$

2.1.3. Autothermal reforming

Autothermal reforming combines partial oxidation and steam reforming. It consists of a thermal zone where partial oxidation or catalytic partial oxidation is used to generate the heat needed to drive the downstream steam reforming reactions in a catalytic zone [7]. No external heating source is required, because the exothermic oxidation reaction provides the heat necessary for the endothermic steam reforming reaction. A significant advantage for this process over steam reforming is that it can be stopped and started very rapidly while producing a larger amount of hydrogen than partial oxidation alone. For autothermal reforming to operate properly both the oxygen to fuel ratio and the steam to carbon ratio must be properly controlled at all times in order to control the reaction temperature and product gas composition while preventing coke formation. For methane reforming the thermal efficiency is comparable to that of partial oxidation reactors 60–70%, based on the higher heating.

2.1.4. Coal Gasification

Coal gasification to produce coal gas dates back to the end of the 18th century. The development of large-scale processes started on the late 1930s. After World War II, interest in coal decreased because of oil and natural gas availability. In 1970s, when oil and natural gas prices increased sharply, interest for coal gasification renewed [19].

Gasification it the only large-scale option for converting solids to gases [20] and one of the most environmentally sustainable conversion technologies for solid fuels. Gasification converts solid fuel into a syngas comprised mainly of CO, CO_2, H_2, CH_4, and H_2O following these reactions [21]:

$$C + \frac{1}{2} O_2 \rightarrow CO \qquad \Delta H^{\circ}_{298} = \text{-111 kJ/mol} \qquad (2.7)$$

$$CO + \frac{1}{2} O_2 \rightarrow CO_2 \qquad \Delta H^{\circ}_{298} = \text{-283 kJ/mol} \qquad (2.8)$$

$$H_2 + \frac{1}{2} O_2 \rightarrow H_2O \qquad \Delta H^{\circ}_{298} = \text{-242 kJ/mol} \qquad (2.9)$$

$$C + CO_2 \rightarrow CO \qquad \Delta H^{\circ}_{298} = \text{172 kJ/mol} \qquad (2.10)$$

$$C + H_2O \rightarrow CO + 2H_2 \qquad \Delta H^{\circ}_{298} = \text{131 kJ/mol} \qquad (2.11)$$

$$C + 2H_2 \rightarrow CH_4 \qquad \Delta H^{\circ}_{298} = \text{-75 kJ/mol} \qquad (2.12)$$

The gasification process takes place at temperatures from 800°C to 1800°C. The exact temperature depends on the characteristics of the feedstock. There is considerable advantage to gasifying under pressure, so that practically all modern processes are operated at pressures of at least 10 bar and up to as high as 100 bar. The reasons are in compression energy savings and equipment size reducing.

2.1.5. Solar Thermolysis

The single-step thermal dissociation of water, known as water thermolysis, can be given as Eq. 13

$$H_2O \rightarrow H_2 + \frac{1}{2} O_2 \qquad \Delta H^{\circ}_{298} = 242 \text{ kJ/mol} \qquad (2.13)$$

The reaction needs a high temperature heat source, above 2500K, to have a reasonable dissociation degree [22]. To reach this temperature, thermal energy of concentrated solar radiation is employed as an energy source. A water thermolysis reactor involves components manufactured with very special refractory materials resistant to reaction ambient, temperatures generally of the order of 1500 K, with gradients and oscillations of relevant magnitude.

Thermal water dissociation can be described by different reactions depending on the temperature. In the temperature range 1700÷1900 K, a heterogeneous reaction (Eq. 14) involving a first-order dissociative reaction localized at the reactor heated wall [23]:

$$H_2O + wall \rightarrow H + OH + wall \qquad (2.14)$$

At higher temperature, in the range of 2000-3000 K, a homogeneous kinetic mechanism with a few reversible elementary steps involving H_2O, OH, H, O, H_2 and O_2 is believed to govern [24].The overall reaction can be expressed as follows:

$$H_2O \rightarrow x_1H_2O + x_2OH + x_3O + x_4H + x_5O_2 + x_6H_2 \qquad (2.15)$$

Thermal water dissociation is an invertible reaction, which is necessary to prevent. Thus, product gas quenching (instant cooling to

stop the reaction) or high-temperature separation of hydrogen should take place in the reactor.

2.2. Hydrogen Storage and Transport

Associated with the above mentioned hydrogen properties, solving storage and transport problems is an important goal to be achieved in the development of the hydrogen economy.

Hydrogen can be stored using different methods that can be subdivided in two groups: physical and chemical methods. Physical storage methods are the high-pressure compression (up to 800 bar) and the liquefaction in cryogenic tank (at 20-21 K). Chemical storage methods include absorption in metal hydrides, adsorption on materials with a large specific surface area, and transformation into other compounds, such as methanol or ammonia. Nowadays the most proven and commercially available hydrogen storage is in gaseous compressed form or in liquid form. However, hydrogen storage methods have several critical features that have to be solved. In general, the weight, volume and cost of hydrogen storage are too high and the durability is not adequate.

References

[1] Van Nostrand R. (2005) *Encyclopedia of Chemistry*, 5th edn, John Wiley & Sons, Inc., Hoboken, NJ, ISBN: 0-471-61525-0

[2] Press R. J., Santhanam K. S. V., Miri M. J., Bailey A. V., Takacs G. A. (2009) *Introduction to Hydrogen Technology*, John Wiley & Sons, Inc, NJ, ISBN: 978-0-471-77985-8

[3] Lai Q., Paskevicius M., Sheppard D. A., Craig E. C. E., Thornton A. W., Hill M. R., Gu Q, Mao J, Huang Z., Liu H. K., Guo Z., Banerjee A., Chakraborty S., Ahuja R., Aguey-Zinsou K.-F. (2015) *Hydrogen Storage Materials for Mobile and Stationary Applications: Current State of the Art*, ChemSusChem, ChemPubSoc Europe, Wiley Online Library, 8, 2789-2825. DOI: 10.1002/cssc.201500231

[4] Cipriani G., Di Dio V., Genduso F., La Cascia D, Liga R., Miceli R., Galluzzo G. R. (2014) *Perspective on hydrogen energy carrier and its automotive applications,* International Journal Of Hydrogen Energy, Elsevier, 39, 8482-8494.

[5] Sharma S., Ghoshal S. K. (2015) *Hydrogen the future transportation fuel: From production to applications,* Renewable and Sustainable Energy Reviews, Elsevier, 43, 1151-1158.

[6] Hosseini S. E., Wahid M. A. (2016) *Hydrogen production from renewable and sustainable energy resources: Promising green energy carrier for clean development,* Renewable and Sustainable Energy Reviews, Elsevier, 57, 850-866.

[7] Holladay J. D., Hu J., King D. L., Wang Y. (2009) *An overview of hydrogen production technologies,* Catalysis Today, Elsevier, 139, 244–260

[8] Acar C., Dincer I. (2014) *Comparative assessment of hydrogen production methods from renewable and non-renewable sources*, International Journal of Hydrogen Energy, Elsevier, 39, 1-12.

[9] Dincer I., Acar C. (2015) *Review and evaluation of hydrogen production methods for better sustainability*, International Journal of Hydrogen Energy, Elsevier, 40, 11094-11111.

[10] French Association of Hydrogen and Fuel Cell (2012) Production d'hydrogene par dissociation de l'eau partir d'un reacteur nucleaire. Memento de l'Hydrogene Fiche 3.2.2, French Association of Hydrogen and Fuel Cell.

[11] Lan R., Irvine J. T. S., Tao S. (2012) *Ammonia and related chemicals as potential indirect hydrogen storage materials*, International Journal of Hydrogen Energy, Elsevier, 37, 1482-1494.

[12] Sherif S. A., Goswami D. Y., Stefanakos E. K., Steinfeld A. (2015) *Handbook of Hydrogen Energy*, CRC Press, Taylor & Francis Group, ISBN-13: 978-1-4200-544-7.

[13] Chorkendorff I., Niemantsverdriet J. W. (2003) *Concepts of Modern Catalysis and Kinetics*, WILEY-VCH Verlag GmbH & Co. KGaA, Weinheim, ISBN: 3-527-30574-2.

[14] Moon D. J. (2008) *Hydrogen Production by Catalytic Reforming of Gaseous Hydrocarbons (Methane & LPG)*, Catal Surv Asia, Springer, 12, 188–202.

[15] Godula-Jopek A., Jehle W., Wellnitz J. (2012) *Hydrogen Storage Technologies. New Materials, Transport and Infrastructure*, Wiley VCH Verlag & co.KGaA, Weinheim, ISBN: 978-527-32683-9.

[16] Iulianelli A., Ribeirinha P., Mendes A., Basile A. (2014) *Methanol steam reforming for hydrogen generation via conventional and*

membrane reactors: A review, Renewable and Sustainable Energy Reviews, Elsevier, 29, 355–368.

[17] Hoogers G. (2003) *Fuel Cell Technology Handbook*, CRC Press, Boca Raton, FL.

[18] Godula-Jopek A. (2015) *Hydrogen Production, by Electrolysis*, Wiley VCH Verlag & co.KGaA, Weinheim, ISBN: 978-3-527-33342-4.

[19] Moulijn J. A., Makkee M., van Diepen A. (2001) *Chemical Process Technology*, John Wiley & Sons, ISBN: 0-471-63009-8.

[20] Rezalyan J., Cheremisinoff N. P. (2005) *Gasification Technologies: A Primer for Engineers and Scientist*, CRC Press, Boca Raton, FL, ISBN: 978-1-4200-2814-0.

[21] Higman C., van der Burgt M. (2008) *Gasificatio*, 2nd edn, Elsevier Science, Oxford, ISBN: 0-7506-7707-4.

[22] Dincer I., Joshi A. S. (2013) *Solar Based Hydrogen Production Systems*, Springer, NY, ISBN: 978-1-4614-7430-2.

[23] Lapicque F., Lédé J., Villermaux J., Cales B., Baumard J. F., Anthony A. M., Abdul-Aziz G., Pnechberty D., Ledoux M. (1985) *Research on the production of hydrogen by direct thermal dissociation of water vapor*, International Journal of Chemical Engineering., 25, 2, 246-257.

[24] Baykara S. Z. (2004) *Experimental Solar Water Thermolysis*, International Journal of Hydrogen Energy, Elsevier, 29, 1459-1469.

3. Fundamental of Electrochemical Water Splitting

3.1. Historical Background

The history of water electrolysis started as early as the first industrial revolution, in the 1800, when Alessandro Volta invented the voltaic pile, and a few weeks later William Nicholson and Anthony Carlisle used it for the electrolysis of water [1]. A few months later, chemist Johann Wilhelm Ritter repeated Carlisle and Nicholson's experiment on electrolysis, succeeding in separating water into hydrogen and oxygen. By 1902 more than 400 industrial water electrolysis units were in operation and in 1939 the first large water electrolysis plant with a capacity of 10,000 Nm^3 H_2/h went into operation. In 1948, the first pressurized industrial electrolyzer was manufactured by Zdansky-Lonza. In 1966, the first solid polymer electrolyte system was built by General Electric, and in 1972 the first solid oxide water electrolysis unit was developed. The first advanced alkaline systems started in 1978. The history ends up in our days with the development of proton exchange membranes, usable for water electrolysis units and fuel cells, by DuPont and other manufacturers, due to the developments in the field of high temperature solid oxide technology and by the optimization and reconstruction of alkaline water electrolyzers [2].

3.2. Thermodynamics of water electrolysis

As mentioned in chapter 2.1, water electrolysis is a hydrogen production method that use electrical energy to split the water molecule in hydrogen and oxygen according to Eq. 3.1

$$H_2O \rightarrow H_2 + \frac{1}{2} O_2 \quad (3.1)$$

At STP, water is liquid and H_2 and O_2 are gaseous. Enthalpy, entropy and free Gibbs energy standard changes for reaction (Eq. 3.1) are, respectively [3]:

$$\Delta H_d^\circ\left(H_2O(l)\right) = +285.84 \text{ kJ/mol} \quad (3.2)$$

$$\Delta S_d^\circ\left(H_2O(l)\right) = +163.15 \text{ J/(mol K)} \quad (3.3)$$

$$\Delta G_d^\circ\left(H_2O(l)\right) = \Delta H_d^\circ\left(H_2O(l)\right) - T\,\Delta S_d^\circ\left(H_2O(l)\right) = +237.22 \text{ kJ/mol} \quad (3.4)$$

The entropy change due to the formation of 1.5 moles of gaseous species is positive along with the enthalpy change so that the Gibbs free energy change is positive and the reaction is non-spontaneous [4].

Water vapor can also be dissociated into gaseous hydrogen and oxygen. Enthalpy, entropy and free Gibbs energy standard changes for reaction with water vapor are respectively:

$$\Delta H_d^\circ\left(H_2O(vap)\right) = +241.80 \text{ kJ/mol} \quad (3.5)$$

$$\Delta S_d^\circ\left(H_2O(vap)\right) = +44.10 \text{ J/(mol K)} \quad (3.6)$$

$$\Delta G_d^\circ\left(H_2O(vap)\right) = \Delta H_d^\circ\left(H_2O(vap)\right) - T\,\Delta S_d^\circ\left(H_2O(vap)\right) = +228.66 \text{ kJ/mol} \quad (3.7)$$

Fig. 3.1 shows the state functions trend for reaction (1) at 1 bar. The total energy ΔH and entropy change ΔS demand to split 1 water mole

are almost constant over the entire temperature range. The Gibbs free energy change ΔG decreases with increasing temperature, while the heat demand TΔS increases linearly with temperature. Discontinuities on ΔH and TΔS observed at 378 K are due to water vaporization.

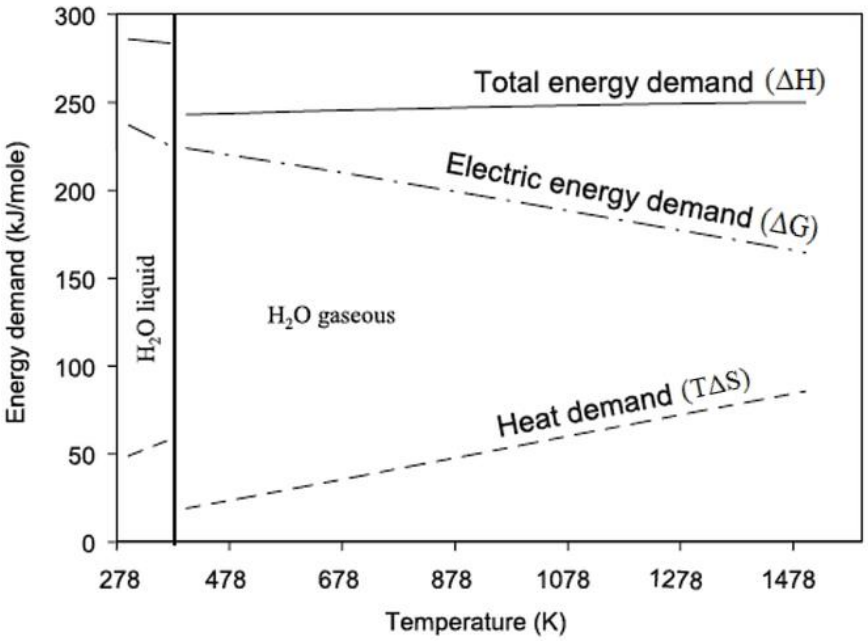

Figure 3.1 – ΔH, ΔG, and TΔS demand for the water splitting reaction at 1 bar [5]

The minimum energy that is required to split water is given by the Gibbs free energy change ΔG. At STP, according to the Faraday's law, the free energy electrolysis in terms of voltage, E°, is, in volts:

$$E^{\circ} = \frac{\Delta G_d^{\circ}}{nF} = 1.2293 \text{ V} \approx 1.23 \text{ V} \quad (3.8)$$

At this cell voltage, there is enough electric energy to start the process but not enough to maintain isothermal conditions. The reaction is

endothermic and the cell takes the thermal energy (TΔS) from the surroundings. Furthermore, the current density is too low, making it not of technological interest. For this reason, the thermo-neutral voltage V° is defined as:

$$V^{\circ} = \frac{\Delta H_d^{\circ}}{nF} = 1.4813 \text{ V} \approx 1.48 \text{ V} \quad (3.9)$$

If the cell voltage is over V°, there are enough electrical and thermal energy to increase the current density to technological acceptable values.

3.3. Electrochemistry of water electrolysis

The aforementioned thermodynamic conditions exist only for low current values, conditions far from the real operating conditions of the cell. In fact, there are several sources of energy dissipation that add up to the energy required for electrolysis. Their magnitude and localization depend on the cell design [4]. Thus, the cell voltage during electrolysis is always higher than E° and it depends on the current through the cell. The overall cell voltage E_{cell} can be written as [6]:

$$E_{cell} = E^{\circ} + iR + |E_{cath}^{ov}| + |E_{an}^{ov}| \quad (3.10)$$

where E_{cath}^{ov} and E_{an}^{ov} are cathodic and anodic reaction overvoltages, which increase logarithmically with current density [7, 8]; iR is the ohmic voltage drop, which is a function of the electrolyte and electrode conductivity, the distance between the electrodes, the conductivity of the diaphragm or the membrane and the contact resistances between the cell components [6].

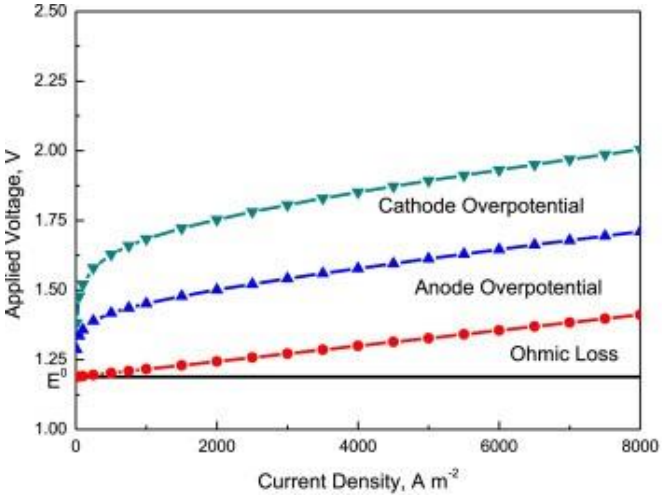

Figure 3.2 – Typical electrolyzer cell losses [9]

3.4. Efficiency

The water electrolysis efficiency is often expressed as the ratio of the energy content of hydrogen produced to the electrical energy consumed for its production (Eq. 11).

$$\eta = \frac{\Delta H_d^{\circ} * n_{H_2,real}}{W_{el}} \tag{3.11}$$

Where n_{H_2} is the amount of hydrogen produced in moles. Eq. 3.11 represents the overall system efficiency that can be further detailed. First, the cell efficiency can be defined as the ratio of either the reversible voltage E° or the thermo-neutral voltage V° to the real cell voltage E_{cell}.

$$\eta_{cell\,\Delta G} = \frac{E^{\circ}}{E_{cell}} \tag{3.12}$$

$$\eta_{cell\,\Delta H} = \frac{V^{\circ}}{E_{cell}} \tag{3.13}$$

These efficiencies refer respectively to the thermodynamic values of maximum work (Eq. 3.12) and maximum thermal energy (Eq. 3.13)

obtainable from the recombination of hydrogen and oxygen and are both decreasing with increasing current.

Another important parameter is the faradic efficiency or current efficiency, which is the ratio of gas produced to the theoretical amount of hydrogen produced according to the electrical charge passed through the cell

$$\eta_{faraday} = \frac{n_{H_2,real}}{n_{H_2,ideal}} \tag{3.14}$$

It takes into account parasitic currents in the cell and possible gases recombination effects. In fact, ideally, cell diaphragm or membrane should be gas-proof. In real condition, the gases solubility in the electrolyte is limited but not zero. The faradic efficiency typically reaches values of over 90 % [10].

References

[1] Santos D. M. F., Sequeira C. A. C., Figueiredo J. L. (2013) *Hydrogen Production by Alkaline Water Electrolysis*, Química Nova, 36, 8, 1176-1193.

[2] Kreuter W., Hofmann H. (1998) *Electrolysis: the Important Energy Transformer in a World of Sustainable Energy*, International Journal of Hydrogen Energy, Pergamon, 23, 8, 661-666

[3] Liu R. S., Zhang L., Sun X., Liu H., Zhang J. (2011) *Electrochemical Technologies for Energy Storage and Conversion*, Wiley-VCH Verlag & Co. KGaA, Boschstr. 12, 69469 Weinheim, Germany, ISBN: 978-3-527-32869-7.

[4] Godula-Jopek A. (2015) *Hydrogen Production, by Electrolysis*, Wiley VCH Verlag & co.KGaA, Weinheim, ISBN: 978-3-527-33342-4.

[5] Hansen J. B. (2015) *Solid oxide electrolysis – a key enabling technology for sustainable energy scenarios*, Faraday Discussions., 182, 9-48.

[6] Zuttel A., Borgschulte A., Schlapbach L. (2008) *Hydrogen as a Future Energy Carrier*, Wiley VCH Verlag & co.KGaA, Weinheim, ISBN: 978-3-527-30817-0.

[7] Wendt H., Imarisio G. (1988) *Nine Years of Research and Development on Advanced Water Electrolysis. A Review of the Research Programme of the Commission of the European Communities*, J. Appl. Electrochem., 18, 1, 1-14.

[8] Wendt H. (1990) *Electrochemical Hydrogen Technologies*, Elsevier, Amsterdam, 1-14.

[9] An L., Zhao T. S., Chai Z. H., Tan P., Zeng L. (2014) *Mathematical modeling of an anion-exchange membrane water electrolyzer for*

hydrogen production, International Journal Of Hydrogen Energy, Elsevier, 39, 35, 19869-19876.

[10] Hug W., Divisek J., Mergel J., Seeger W., Steeb H. (1992) *Highly efficient advanced alkaline electrolyzer for solar operation*, International Journal Of Hydrogen Energy, Elsevier, 17, 9, 699-705.

4. Water Electrolysis Technologies

Nowadays, there are three technologies through which water electrolysis can be carried out: i) alkaline water electrolysis (AWE), ii) polymer electrolyte membrane (PEM) electrolysis, ad iii) solid oxide electrolysis cell (SOEC). Alkaline and PEM electrolysis are both mature technologies already commercialized while SOECs are still developing.

A typical electrolysis cell consists of two electrodes, a diaphragm or a membrane, an electrolyte, and an external power sources.

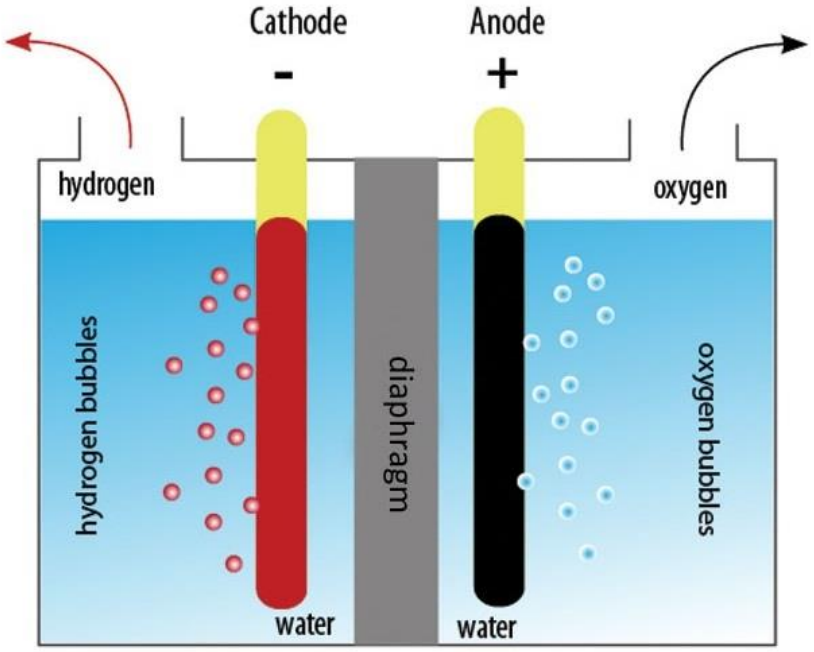

Figure 4.1 – Typical scheme of an electrolysis cell.

The main characteristics of the different types of electrolyzers will be illustrated below.

4.1. Alkaline Water Electrolysis

Alkaline electrolysis is the most mature and the most developed water electrolysis technology. Most of the global electrolytic hydrogen is produced by alkaline electrolyzers. Commercial alkaline electrolyzers have a typical energy efficiency of 60-70 %, and a lifetime up to 90-100,000 operation hrs. [1-3]. They use typically a 20-40 % potassium hydroxide (KOH) aqueous solution at a temperature ranging from 60-90 °C [1, 4-6]. One of the strengths of the technology is the use of electrodes made with inexpensive materials such as Nickel [7-10].

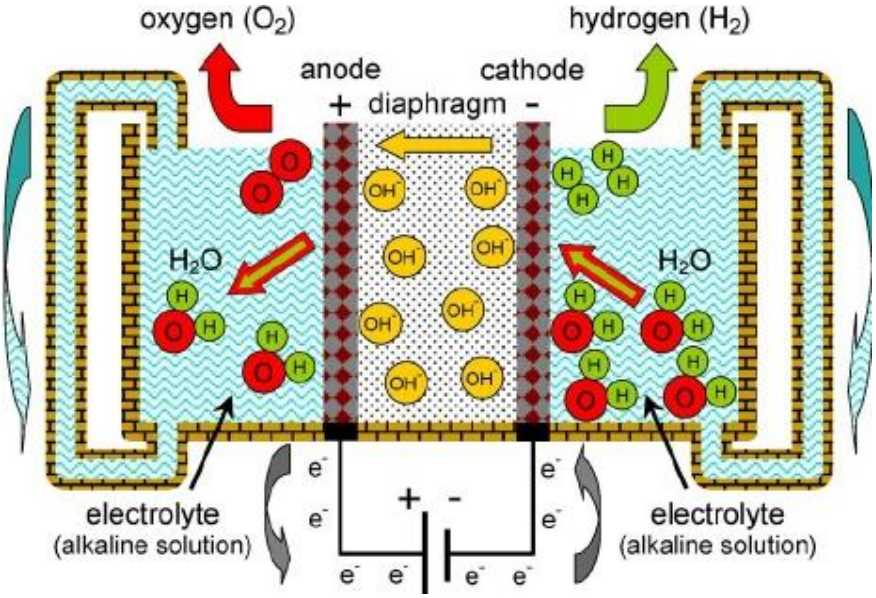

Figure 4.2 – Scheme of an alkaline electrolysis cell [11]

As shown in Fig 4.2, hydrogen evolution occurs at the cathode, where water is reduced (Eq. 4.1). Crossing the diaphragm (or the membrane), the hydroxide anions recombine on the anode surface according to Eq. 4.2, where water and oxygen are formed.

Cathode: $4H_2O + 4e^- \rightarrow 2H_2 + 4OH^-$ (4.1)

Anode: $4OH^- \rightarrow O_2 + 2H_2O + 4e^-$ (4.2)

Full reaction: $2H_2O \rightarrow 2H_2 + O_2$ (4.3)

The diaphragm separates the gases, avoiding their recombination, but guarantees the liquid continuity. In the past, the AWE diaphragms were made of asbestos [12-13]. Nowadays, they are based on sulphonated polymers, Polyphenylene Sulfide (Ryton®) [14], and composite materials [15-16]. One of the most popular material used a separator is known as Zirfon®, a composite material made of polysulphone and zirconium oxide.

In recent years, significant progress has been made regarding alkaline electrolysis mainly in two directions. On the one hand, the energy efficiency of the electrolyzers has been improved with the aim of reducing the operating costs associated with the consumption of electricity, improving both the electrodes electrocatalytic activity [17-22] and the design of the cell [23-24]; on the other hand, operating current densities have been increased in order to reduce investment costs [25]. In addition, advanced alkaline electrolyzers operating at high temperature and high pressure are under study [26-28]. These systems are able to reach current densities of 1-2 A cm^{-2} with cell voltage lower than 2 V, but they operate at temperatures of 250 °C and 42 bar. These conditions require energy to be maintained and deteriorate the materials used.

4.2. PEM Water Electrolysis

PEM electrolysis is similar to AWE. Fig. 4.3 shows a PEM cell diagram.

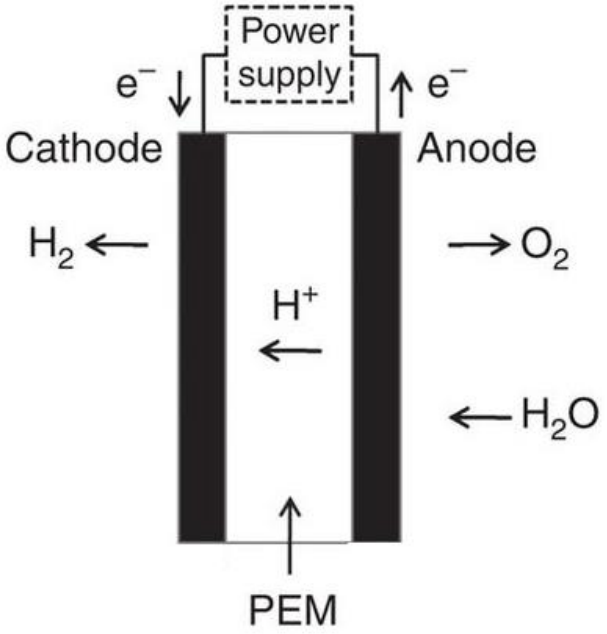

Figure 4.3 – Scheme of a PEM Electrolysis cell [29].

The substantial difference between AWE and PEM electrolysis is the electrolyte nature. Instead of an aqueous electrolyte like in AWE cells, PEM cell electrolyte is an acidic solid polymer membrane, typically Nafion™. This membrane performs two tasks: i) separates the gases produced, and ii) allows the proton flux from the anode to the cathode. The proton transfer is due to the presence in the membrane of the sulphonic acid functional group ($-SO_3H$) [30]. Being in an acid environment, the electrode reactions of a PEM cell are different from

those of an AWE cell. At the anode, oxidation reaction of deionized water (Eq. 4.4) occurs. Through the membrane, hydrogen ions reach the cathode and form hydrogen gas (Eq. 4.5).

Anode: $2H_2O \rightarrow O_2 + 4H^+ + 4e^-$ (4.4)

Cathode: $4H^+ + 4e^- \rightarrow 2H_2$ (4.5)

The global reaction is the same as reported in Eq. 4.3. The use of deionized water is necessary because noble metals, such as platinum and iridium, which are easily poisoned by impurities, are used as electro-catalysts.

In terms of temperature and pressure, the operating conditions of a PEM cell are similar to the alkaline ones. However, the current densities of a PEM cell can reach values of 2 Acm^{-2} without significant losses in efficiency [3]. This is due to the thin assembly between the electrode and the membrane (<0.2 mm), named membrane electrode assembly (MEA), which minimizes the cell ohmic losses.

The main disadvantage of PEM electrolysis is the high investment cost due to the use of noble metals as catalysts. For the same reason, PEM electrolyzers are made with lower production capacity than alkaline ones. Furthermore, they have a shorter life time.

4.2.1. PEM Water Electrolysis Tests at NREL

During the abroad experience in Colorado at NREL, five commercial MEAs were tested for a Round Robin Test with other research institutes and companies. For the tests, a cell with the following characteristics was used:

- Cathode Flow-Field: Titanium coated with Platinum and Gilded

- Anode Flow-Field: Titanium coated with Platinum
- End-Plates: $AlMg_3$
- Active Area: 25 cm^2
- PTL: Toray-Paper 5% PTFE, thickness: 0.35 mm
- Gaskets: PTFE, thickness: 0.25 mm

The tests operation conditions were:

- Water Flow: 2 mL/(min*cm^2)
- Outlet pressure: 1 bar
- ΔT (inlet-outlet) $\leq$ 2 K
- Water quality > 1 MΩ*cm

The purpose of the tests was to obtain polarization curves at two different temperatures, 60 and 80 ° C, and verify their repeatability for all MEAs. The polarization curves were obtained by keeping the constant current for 5 minutes for each current step. Figures 4.4 and 4.5 show the polarization curves for 60 and 80 °C respectively.

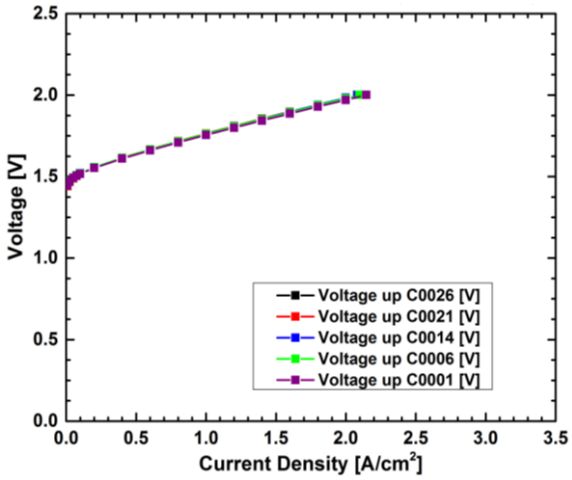

Figure 4.4 – Polarization curve for five commercial MEAs tested in a PEM electrolyzer at 60 °C. Tests conducted at NREL.

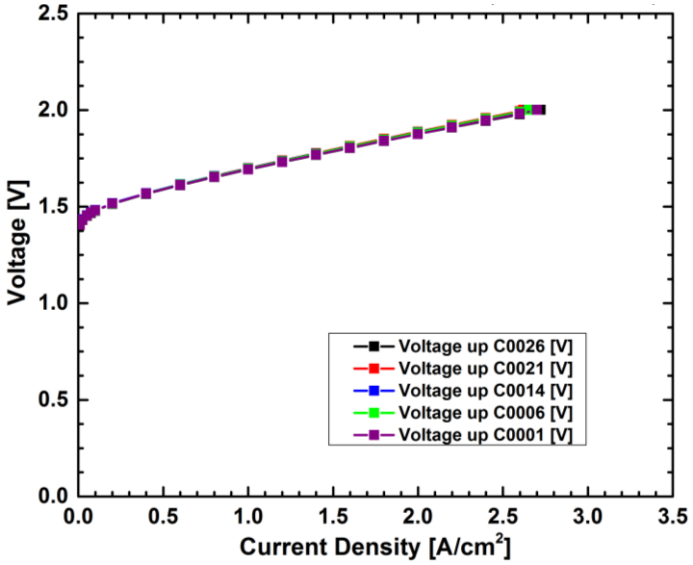

Figure 4.5 – Polarization curve for five commercial MEAs tested in a PEM electrolyzer at 80 °C. Tests conducted at NREL.

The results obtained were excellent, showing a high repeatability at both temperatures. It is important to underline that at the upper voltage limit value (2 V) the difference in current density between the two temperatures is about 0.6 A/cm^2, strongly marking the effect of temperature in the electrolysis reaction.

4.3. Solid Oxide Electrolysis Cell

Solid oxide electrolysis cell is the least mature electrolysis technology, despite being a technology already investigated since the 1960s [11]. The electrolyte for SOEC is a ceramic material, where oxygen ions at high temperatures act as electrical charge carriers. The operating temperature for these cells is typically 700-1000 ° C, working with water vapor phase. The main advantage of the SOECs lies in the low

electrical energy demand for the gas production, replaced by heat [31]. However, having to withstand high temperatures, the materials and fabrication methods of cell are expensive. As mentioned, the electrolyte is a ceramic material, typically yttria stabilized zirconia (YSZ) [7]. The cathode is a cermet, i.e. a mixture of Ni and YSZ, while anode is typically a strontium-doped perovskite, such as $LaMnO_3$, $LaFeO_3$ or $LaCoO_3$ [32-33]. Fig. 4.6 shows the operating principle for SOEC.

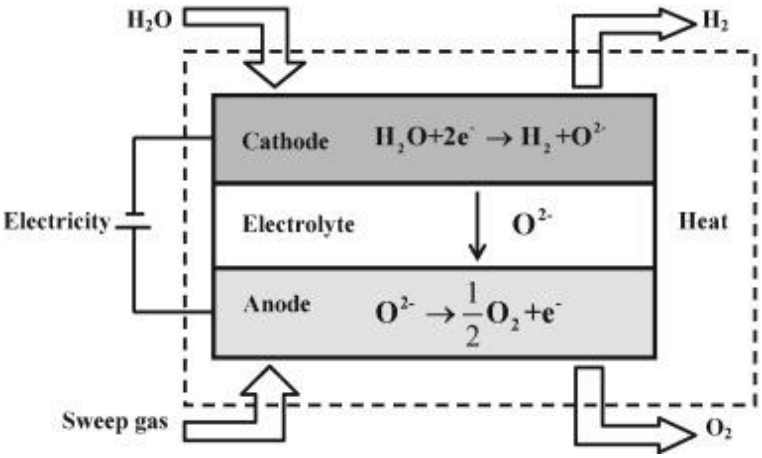

Figure 4.6 – Scheme of a SOEC Cell [34].

At the cathode side, water steam is reduced in H_2 and oxide ion (O^{2-}), according to Eq. 4.6. Through the electrolyte, the anions reach the anode and react to form oxygen gas (Eq. 4.7).

Cathode: $$2H_2O + 4e^- \rightarrow 2H_2 + 2O^{2-} \quad (4.6)$$

Anode: $$2O^{2-} \rightarrow O_2 + 4e^- \quad (4.7)$$

The main drawback is the low performance stability due to the degradation of the electrodes due to the high temperatures. In some recent

studies, single cells have reached lifetimes of 11,000 [35] and 23,000 [36] hrs. Instead, data on small stacks refer to 4000 operation hrs. [37].

References

[1] Rand D. A. J., Dell R. M. (2007) *Hydrogen Energy: Challenges and Prospects*, Royal Society of Chemistry Energy Series.

[2] Gandía L. M., Arzamendi G., Diéguez P. M. (2013) *Renewable Hydrogen Technologies. Production, Purification, Storage, Applications, and Safety*, Elsevier, Amsterdam.

[3] Carmo M., Fritz D. L., Mergel J., Stolten D. (2013) *A Comprehensive Review on PEM Water Electrolysis*, International Journal of Hydrogen Energy, Elsevier, 38, 12, 4901-4939.

[4] Zuttel A., Borgschulte A., Schlapbach L. (2008) *Hydrogen as a Future Energy Carrier*, Wiley VCH Verlag & co.KGaA, Weinheim, ISBN: 978-3-527-30817-0.

[5] Zeng K., Zhang D. (2010) *Recent Progress in Alkaline Water Electrolysis for Hydrogen Production and Applications*, Progress in Energy and Combustion Science, 36, 3, 307-326.

[6] Dyer C. K., Moseley P. T., Ogumi Z., Rand D. A. J., Scrosati B. (2013) *Encyclopedia of Electrochemical Power Sources*, Newnes.

[7] Lehner M., Tichler R., Steinmüller H., Koppe M. (2014) *Power-to-Gas: Technology and Business Models*, Springer International Publishing, New York.

[8] Rebak R. B. (2000) *Nickel Alloys for Corrosive Environments*, Advanced Materials and Processes, 157, 2, 37-42.

[9] Janjua M. B. I., Le Roy R.L. (1985) *Electrocatalyst performance in industrial water electrolysers*, International Journal Of Hydrogen Energy, 10, 1, 11-19.

[10] Gong M., Wang D.-Y., Chen C.-C., Hwang, B.-J., Dai H. (2016) *A Mini Review on Nickel-Based Electrocatalysts for Alkaline Hydrogen Evolution Reaction,* Nano Research, 9 (1), 28-46.

[11] Ursùa A., Gandìa L. M., Sanchis P. (2012) *Hydrogen Production from Water Electrolysis: Current Status and Future Trends*, Proceedings of the Institute of Electrical and Electronics Engineers, 100, 2, 410-426.

[12] Gallone P. (1973) *Trattato di ingegneria elettrochimica*, Tamburini Editore, Milan.

[13] McAuliffe T. R. (1980) *Hydrogen and Energy*, Macmillan Press Ltd., London.

[14] Irving L. R. (1986) Treadwell Corp (US). US Patent, 4707228, 1986-11-17.

[15] Vermeiren P. H., Leysen R., Beckers H., Moreels J. P., Claes A. (2008) *The influence of manufacturing parameters on the properties of macroporous Zirfon® separators*, Journal of Porous Materials, 15, 3, 259-264.

[16] Xu L., Li W., You Y., Zhang S., Zhao Y. (2013) *Polysulfone and zirconia composite separators for alkaline water electrolysis*, Frontiers of Chemical Science and Engineering, 7, 2, 154-161.

[17] Rafailovic L. D., Gammer C., Rentenberger C., Trisovic T., Kleber C., Karnthaler H. P. (2013) *Enhanced oxygen evolution and reduction reactions of porous ternary NiCoFe foam electrodes prepared by dynamic hydrogen template deposition*, Nano Energy, Elsevier, 2, 523-529.

[18] Rosalbino F., Delsante S., Borzone G., Scavino G. (2013) *Electrocatalytic activity of crystalline Ni-Co-M (M = Cr, Mn, Cu) alloys*

on the oxygen evolution reaction in an alkaline environment, International Journal of Hydrogen Energy, Elsevier, 38, 10170-10177.

[19] Battaglia M., Inguanta R., Piazza S., Sunseri C. (2014) *Fabrication and characterization of nanostructured Ni-IrO2 electrodes for water* electrolysis, International Journal of Hydrogen Energy, Elsevier, 39, 16797-16805.

[20] Hong S. H., Ahn S. H., Choi I., Pyo S. G., Kim H. J., Jang J. H., Kim S. K. (2014) *Fabrication and Evolution of Nickel Cobalt Alloy Electrocatalysts for Alkaline Water Splitting*, Applied Surface Science, 307, 146-152.

[21] Lupi C., Dell'Era A., Pasquali M. (2014) *In Situ Activation with Mo of Ni-Co Alloys for Hydrogen Evolution Reaction*, International Journal of Hydrogen Energy, Elsevier, 39, 1932-1940.

[22] Cardoso D. S. P., Amaral L., Santos D. M. F., Sljukic B., Sequeira C. A. C., Macciò D., Saccone A. (2015) *Enhancement of Hydrogen Evolution in Alkaline water Electrolysis by using Nickel-Rare earth Alloys*, International Journal of Hydrogen Energy, Elsevier, 40, 4295-4302.

[23] Phillips R., Edwards A., Rome B., Jones D. R., Dunnill C. W. (2017) *Minimising the ohmic resistance of an alkaline electrolysis cell through effective cell design*, International Journal of Hydrogen Energy, 42, 23986-23994.

[24] Phillips R., Dunnill C. W. (2016) *Zero Gap Alkaline Electrolysis Cell Design for Renewable Energy Storage as Hydrogen Gas*, Royal Society of Chemistry Advances, 6, 100643-100651.

[25] Li X., Walsh F. C, Pletcher D. (2011) *Nickel based electrocatalysts for oxygen evolution in high current density, alkaline water electrolysers*, Physical Chemistry Chemical Physics, 13, 1162-1167.

[26] Vandenborre H., Leysen R., Nackaerts H., Van Asbroeck P. (1984) *A survey of five year intensive R&D work in Belgium on advanced alkaline water electrolysis*, International Journal of Hydrogen Energy, 9, 277-284.

[27] Ganley J. C. (2009) *High temperature and pressure alkaline electrolysis*, International Journal of Hydrogen Energy, 34, 3604-3611.

[28] Allebrod F., Chatzichristodoulou C. , Mogensen M. B. (2013) *Alkaline electrolysis cell at high temperature and pressure of 250 °C and 42 bar*, Journal of Power Sources, 229, 22-31.

[29] Chen Y. X., Lavacchi A., Miller H. A., Bevilacqua M., Filippi J., Innocenti M., Marchionni A., Oberhauser W., Wang L., Vizza F. (2014) *Nanotechnology makes biomass electrolysis more energy efficient than water electrolysis*, Nature Communications, 5:4036, 1-6.

[30] Larminie J., Dicks A. (2003) *Fuel Cell Systems Explained*, Wiley, Chichester.

[31] Godula-Jopek A. (2015) Hydrogen Production, by Electrolysis, Wiley VCH Verlag & co.KGaA, Weinheim, ISBN: 978-3-527-33342-4.

[32] Hong H. S., Ui-Seok Chae U. S., Choo S. T., Lee K. S. (2005) *Microstructure and electrical conductivity of Ni/YSZ and NiO/YSZ composites for high-temperature electrolysis prepared by mechanical alloying*, Journal of Power Sources, 149, 84–89.

[33] Kong J., Zhang Y., Deng C., Xu J. (2009) *Synthesis and electrochemical properties of LSM and LSF perovskites as anode*

materials for high temperature steam electrolysis, Journal of Power Sources, 186, 485-489.

[34] Im-orb K., Visitdumrongkul N., Saebea D., Patcharavorachot Y., Arpornwichanop A. (2018) *Flowsheet-based model and exergy analysis of solid oxide electrolysis, cells for clean hydrogen production*, Journal of Cleaner Production, 170, 1-13.

[35] Schefold J., Brisse A., Poepke H. (2015) *Long-term Steam Electrolysis with Electrolyte-Supported Solid Oxide Cells*, Electrochemical Acta, 179, 161-168.

[36] Schefold J., Brisse A., Poepke H. (2017) *23,000 h steam electrolysis with an electrolyte supported solid oxide cell*, International Journal of Hydrogen Energy, 42, 13415-13426.

[37] Schefold J., Brisse A., Zahid M., Ouweltjes J. P., Nielsen J. U.(2011) *Long term testing of short stacks with solid oxide cells for water electrolysis*, Electrochemical Society Transactions, 35, 1, 2915-2927.

5. Nanostructures Fabrication

Over the last decades, the ever-increasing demand for more efficient materials led to the production of different materials such as metal alloys, oxides, and polymeric materials. In this frame, growing attention has been devoted to the nanostructured materials, which they are characterized by having at least one dimension ranging from 1 nm to 100 nm. This is in good agreement on how the term “nano” is used in the scientific community, though there is a degree of ambiguity in relation to the upper limit of the size. Particles and materials with the smallest domain between sizes above one micron and even sometimes several μm are sometimes referred to as “nano”, although this is becoming less common with increasing standardization of terminology in nanoscience. Nanostructures can have a great variety of shapes. Generally, the easiest to realize are one-dimensional (1D) ones, such as wires, rods, belts, and tubes. The academic and industrial interest for nanostructured materials is due to the specific electrical, electrochemical, optical, and magnetic characteristics. There are many different applications where nanostructures are already used and where their use is foreseen:

- Nanomedicine;
- Catalysis and filtration;
- Energy conversion and storage;
- Semiconductor and optoelectronic devices;
- Sensing.

This large number of applications is also due to the variety of possible methods for the nanostructure fabrication. Usually, fabrication methods are classified as “bottom-up” or “top-down”. The first one

includes the most common fabrication methods [1]: i) template synthesis [2-5], ii) vapor-solid growth [6-8], iii) vapor-liquid-solid (VLS) growth [9-11], iv) hydrothermal [12, 13], v) solvothermal [14-15], vi) electrochemical deposition [16-19]. The second one includes all the nanolithographic techniques [20, 21]: i) electron-beam [22], ii) focused-ion-beam [23] writing, iii) proximal-probe patterning [24], iv) X-ray and v) extreme-UV lithography [25-26].

In this work, the attention is focused on the materials synthesized through deposition into template, which has been used as electrodes for water splitting after template removing.

5.1. Synthesis through Template

Synthesis through a template is an easy and extensively used method for 1D nanostructures fabrication [1, 16]. In this approach, the template serves to give the desired form to nanostructures; therefore it is easy to manage the size and shape of the nanostructures by choosing the proper template.

Fig. 5.1 shows the nanostructures growing process step-by-step for each template type. The most common template types are planar and colloidal ones, and both are divided into porous and nonporous [27]. In particular, the use of porous planar templates permits the preparation of materials with well-defined three-dimensional morphologies. Usually, a porous planar template is a material that has pores with radii varying from tens of nm to a few μm. These are often used as membranes in filtration technology. Anodic aluminum oxide membrane [5, 16, 19, 28] and polycarbonate membrane [29-36] are commonly used for the

synthesis of 1D nanostructures, which are often nanotubes or nanowires (NWs).

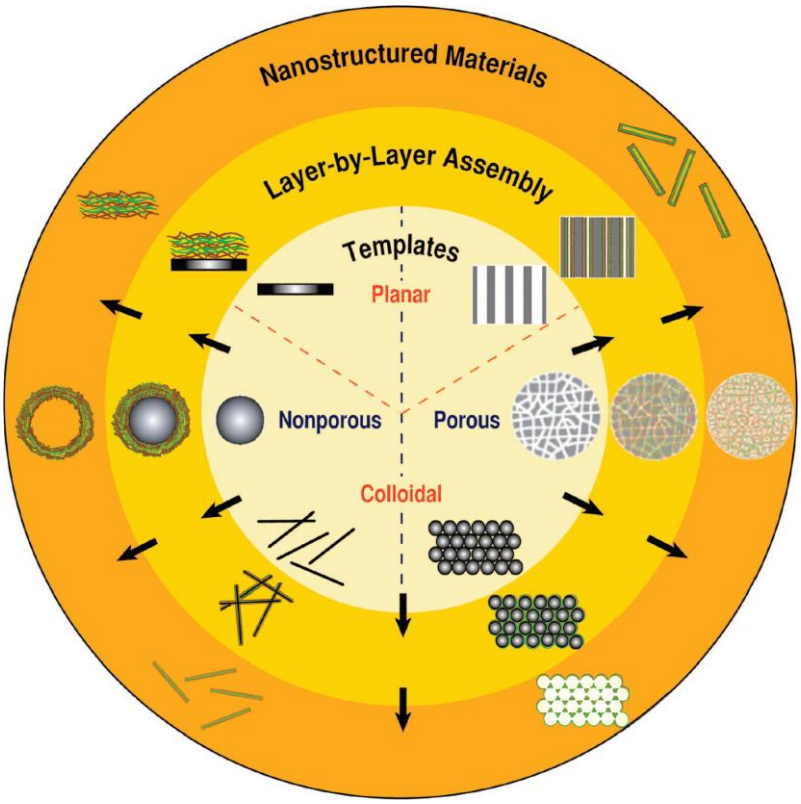

Figure 5.1 – Schematic illustration of various nanostructured materials prepared via templating technique [27].

For this work, commercially track-etched polycarbonate membranes (Whatman, Cyclopore 47) were used as a template with pore diameter ranging from 180 to 250 nm, pore density of 10^{12} pores m^{-2}, and

a thickness of about 16 ± 0.65 μm. A typical morphology is shown in Fig. 5.2.

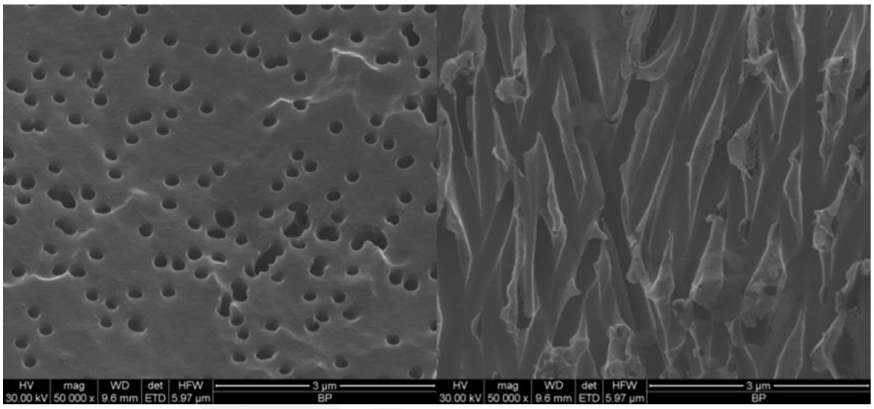

Figure 5.2 – Polycarbonate Membrane SEM images: left) top view; right) section view

The main advantages in using the polycarbonate membrane are the high density of highly interconnected pores and the ease of dissolution. Further, after dissolution, it is possible to recover the polycarbonate from either dichloromethane or chloroform, which are used as etching agents.

5.2. Electrochemical Deposition

Electrochemical deposition is a process which involves the reduction of metal from aqueous, organic, and fused-salt electrolytes [17, 37]. The reduction of metal ions (M^{z+}) in aqueous solution can be accomplished by three different processes: i) electrodeposition, ii) electroless deposition, and iii) displacement deposition. For the first two processes, metal reduction reaction is represented by Eq. 5.1.

$$M^{z+}_{solution} + ze^- \rightarrow M_{lattice} \quad (5.1)$$

In the electrodeposition process, the electrons needed for the reaction are provided by an external power supply. While for the electroless deposition, the electrons source is a reducing agent present in the solution. In the displacement deposition, the electrons needed for the reduction of metal ions (M_a^{z+}) present in the solution are provided from the oxidation of metal substrate (M_b), which behaves as a sacrificial anode, according to the partial reactions

Oxidation: $M_b \rightarrow M_b^{z+} + ze^-$ (5.2)

Reduction: $M_a^{z+} + ze^- \rightarrow M_a$ (5.3)

Giving the resultant reaction

$$M_a^{z+} + M_b \rightarrow M_a + M_b^{z+} \quad (5.4)$$

Among the processes listed above, the most one widely used is electrodeposition. Electrodeposition process shows many advantages over physical and chemical deposition methods, such as i) no need of vacuum equipment, ii) easy handling, iii) higher deposition rates with also a high surface area, and iv) easy preparation of thick and continuous layers firmly attached to the support. Other advantages include the ease of fabrication, low cost, sample homogeneity and precise control over the amount of electrodeposited material. Furthermore, electrochemical deposition methods are often compatible with other fabrication techniques such as sputtering, evaporation processes or photolithography. The electrodeposition requires the use of a rather simple apparatus (Fig. 5.3):

- a potentiostat for setting the potential or the current;
- a working electrode (WE), where deposition occurs;
- a counter-electrode;
- a reference electrode, which allows applying the desired potential to WE.
- a solution, containing the precursor salts of the elements to be deposited.

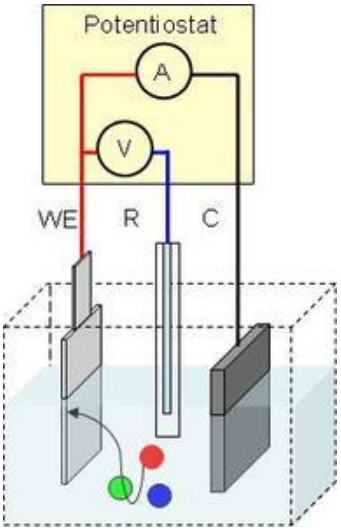

Figure 5.3 – Elementary scheme of an electrodeposition system

Shortly, the electrodeposition process involves external polarization of the WE. As the current passes throughout the cell, an oxidation reaction occurs at the anode (counter-electrode) while a reduction reaction takes place on the cathode (working electrode), with deposition of the desired material.

Numerous chemical and operational parameters must be controlled for conducting successfully electrodeposition; such as current

density, electrolyte concentration, complexing agent, pH, temperature, electrolyte stirring, substrate properties, cleaning procedure. In addition, working electrode can be polarized through current density or potential; consequently, the deposition process can be carried out through potentiostatic, constant current, cyclic voltammetry, pulsed potential, or square current polarization. The technique choice is related to the electrochemical behavior of the desired material.

5.3. Template Electrosynthesis

In this work, template electrosynthesis was chosen for the nanostructured electrode fabrication, because is easy to be conducted, cheap, and easily scalable. In addition, like all electrochemical-based processes, it is environmentally friendly because electron is a reagent. Fig. 5.4 shows a schematic diagram for the synthesis of nanostructures through electrodeposition.

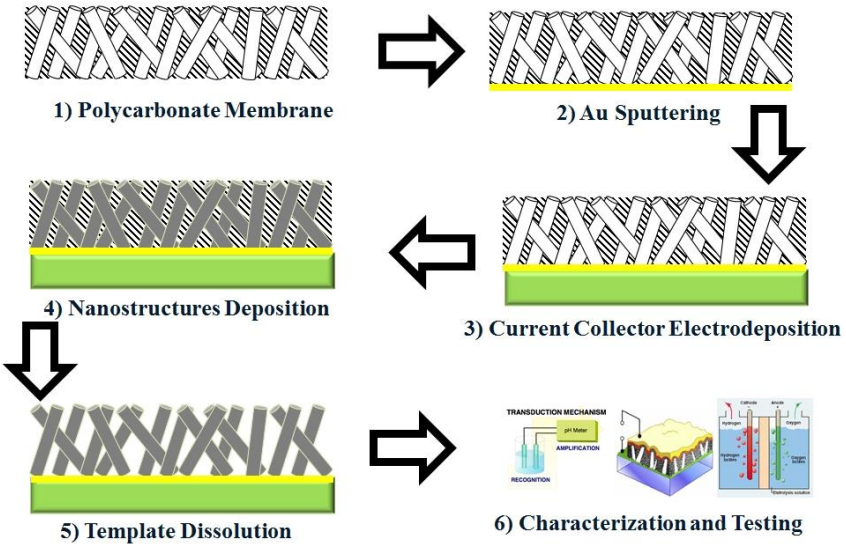

Figure 5.4 – Process steps for electrodeposition into template.

The details for each type of electrode will be shown in the following chapters. As mentioned above, a porous polycarbonate membrane was used as a template, since it is not electrically conductive; a gold film 20-30 nm thick was sputtered on one side of the membrane. The gold sputtering was made with a SCANCOAT SIX EDWARDS. During the sputtering, the chamber pressure was 10^{-1} mbar and, inside the chamber, there was an Argon atmosphere; the potential and current values were 1 kV and 25 mA respectively for 240 s. Successively, a compact Ni layer was electrodeposited on the golden surface. The Ni layer acted as current collector and mechanical support of the nanostructures, and it was deposited from a typical Watt's bath (300 g/l nickel sulphate hexahydrate, 45 g/l nickel chloride, 45 g/l boric acid) at 3 pH.

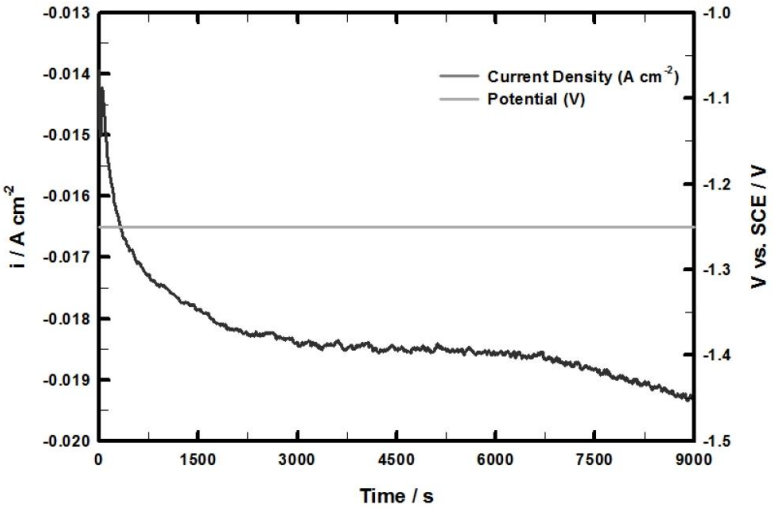

Figure 5.5 - Ni layer electrodeposition potential and current density vs. time.

The working electrode was potentiostatically polarized at -1.25 V Vs. a standard calomel electrode (SCE), while a platinum gauze was used as a counter-electrode. Under these conditions, the Ni layer deposited after 9000 seconds was 80 μm thick. Fig. 5.5 shows a typical current density vs. time plot during the Ni film deposition. The electrodeposited Ni layer was successively used as a current collector for electrodepositing the nanostructures into the template. Due to the cylindrical shape of the pores, usually the nanostructures were NWs. After the nanostructures growth, the template was dissolved in dichloromethane. The electrode was immersed in the fresh dissolving agent for 5 minutes, and the procedure was repeated four times to guarantee complete dissolution of the membrane. Then, the electrodes were morphologically, chemically and electrocatalytically characterized.

5.3.1. Ni NWs Fabrication

Initially, anodic alumina membrane was used as a template [19], but successively, it was substituted with polycarbonate membrane, because the alkaline solution for dissolving alumina membrane damaged the deposited NWs. Consequently track-etched polycarbonate membranes were selected [39], because easily dissolve into organic compound. Moving from these initial results, the electrodeposition technique has been further optimized, especially in terms of deposition time.

Starting from a membrane with a Ni layer, Ni nanowires were electrodeposited into the membrane pores through a triangular pulsed potential between - 0.3 and -1.25 V vs. SCE with a slope of 0.1 Vs^{-1}, for 90 pulses, and frequency of 0.053 Hz. A platinum grid was used as a counter-electrode, while a Watts's bath identical to that one used for

deposition of the current collector was used as an electrolyte. Fig. 5.6 shows the shape of the applied potential and current density response.

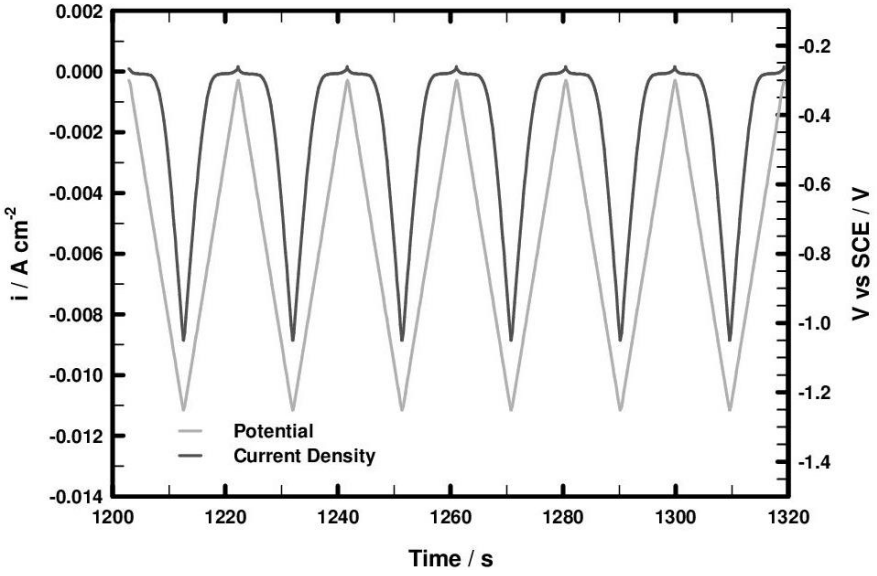

Figure 5.6 – Potentiostatic applied potential and passing current density vs. time for Ni NWs electrodeposition. Ni NWs were growth up for 90 pulses from -0.3 V to -1.25 V vs. SCE (scan rate 0.1 Vs-1)

The current response varied between 0.0 and -0.009 Acm^{-2} at the same frequency of the potential. In addition, the current density was practically null at potential more anodic than -0.7 V vs. SCE, where a plateau starts and a small anodic spike is present in correspondence of the applied potential inversion. The absence of any current at the potential plateau indicates that likely there is not hydrogen evolution simultaneously to NWs deposition. At the Watt's bath pH, the thermodynamic potential for hydrogen evolution is -0.177 V vs. NHE [38] equal to -0.419 V vs. SCE, therefore at a potential more anodic than

-0.419 an oxidation current of H_2 was expected at potential lower than -0.419 V vs SCE if hydrogen evolution occurred according the reaction

$$H_2 \rightarrow 2H^+ + 2e^- \quad (5.5)$$

The absence of such a current supports the conclusion that faradic efficiency for fabrication of Ni NWs was practically unitary.

5.3.2. Ni NWs + Pd Nanoparticles Fabrication

After dissolution of the template, Pd nanoparticles were deposited on Ni NWs surface through a displacement reaction where the same Ni NWs is the oxidizing metal. The deposition was conducted in a 5mM $Pd(NH_3)_4(NO_3)_2$ aqueous solution with 0.1 M H_3BO_3 at room temperature. Solution was acidified using HNO_3 to shift the pH to 2 and sonicated during the deposition. Upon immersion of Ni NWs into electrolyte, deposition of Pd nanoparticles onto Ni NWs surface was observed, owing to the simultaneous partial reactions

$$Pd(NH_3)_4^{2+} + 2e^- + 4H_2O = Pd + 4NH_4^+ + 4OH^- \quad E° = 0.0 \text{ V (NHE)} \quad (5.6)$$

$$Ni \rightarrow Ni^{2+} + 2e^- \quad E^0 = -0.257 \text{ V (NHE)} \quad (5.7)$$

During deposition, pH was increasing owing to the side cathodic reaction involving nitrate ions and driven by reaction Eq. 5.8 [5, 35]:

$$NO_3^- + H_2O + 2e^- \rightarrow NO_2^- + 2OH^- \quad E^0 = 0.01 \text{ V (NHE)} \quad (5.8)$$

In order to examine the deposition over time, tests were performed at 1, 5, and 10 minutes.

5.3.3. Pd NWs Fabrication

For comparison, Pd NWs were also fabricated through a displacement deposition from a 5 mM $Pd(NH_3)_4(NO_3)_2$ solution at pH 2 for 1 hr. Usually, an aluminum strip was used as a sacrificial anode, with cathodic to anodic surface ratio equal to 0.065 [35].This ratio is a fundamental parameter for controlling the rate of deposition. The anodic reaction was

$$Al \rightarrow Al^{3+} + 3e^{-} \qquad E^0 = -1.7 \text{ V (NHE)} \qquad (5.9)$$

The scheme of the galvanic connection is shown in Fig. 5.7.

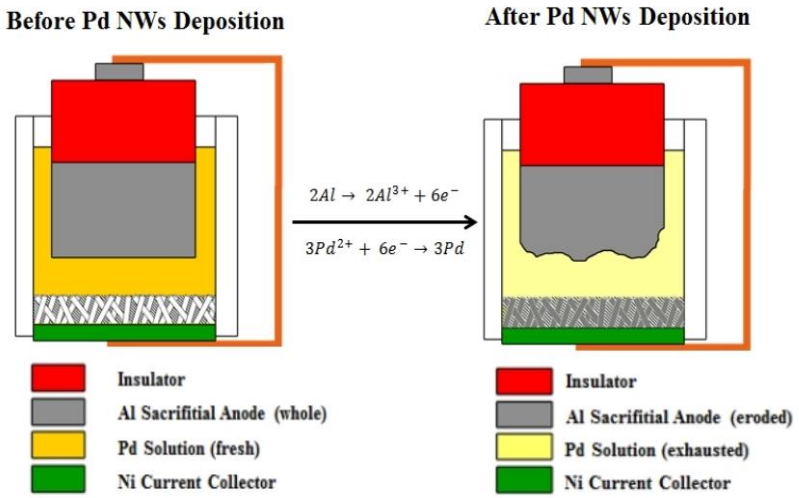

Figure 5.7 – Scheme of the galvanic connection for Pd NWs deposition

During the Pd NWs deposition, the solution color changed from the initial dark yellow to transparent after the deposition; this behavior was maybe due to pH change and to Pd solution discharge.

References

[1] Xia Y., Yang P., Sun Y. Wu Y., Mayers B., Gates B., Yin Y., Kim F., Yan H. (2003) *One-Dimensional Nanostructures: Synthesis, Characterization, and Applications*, Advanced Materials, Wiley-VCH, 15, 353-389.

[2] Ringsdorf H., Schlarb B., Venzmer J. (1988) *Molecular Architecture and Function of Polymeric Oriented Systems: Models for the Study of Organization, Surface Recognition, and Dynamics of Biomembranes*, Angewandte Chemie International Edition, 27, 113–158.

[3] Obare S. O., Jana N. R., Murphy C. J. (2001) *Preparation of Polystyrene- and Silica-Coated Gold Nanorods and Their Use as Templates for the Synthesis of Hollow Nanotubes*, Nano Letters, 1, 601-603.

[4] Mayya K. S., Gittins D. I., Dibaj A. M., Caruso F. (2001) *Nanotubes Prepared by Templating Sacrificial Nickel Nanorods*, Nano Letters, 1, 727-730.

[5] Inguanta R., Piazza S., Sunseri C. (2009) *Synthesis of self-standing Pd nanowires via galvanic displacement deposition*, Electrochemistry Communications, 11, 7, 1385-1388.

[6] Levitt A. P. (1970) *Whisker Technology*, Wiley-Interscience, New York.

[7] Strelcov E., Davydov A. V, Lanke U., Watts C., Kolmakov A. (2011) *In Situ Monitoring of the Growth, Intermediate Phase Transformations and Templating of Single Crystal VO2 Nanowires and Nanoplatelets*, American Chemical Society Nano, 5, 4, 3373–3384.

[8] Cheng Y., Zhang T., Cai Y., Ho K. M., Fung K. K., Wang N. (2010) *Structure and Metal-to-Insulator Transition of VO2Nanowires Grown on*

Sapphire Substrates, European Journal of Inorganic Chemistry., 27, 4332-4338.

[9] Wagner R. S., Ellis W. C. (1964) *Vapor-Liquid-Solid Mechanism Of Single Crystal Growth*, Applied Physics Letters, 4, 89.

[10] Duan X., Lieber C. M. (2000) *General Synthesis of Compound Semiconductor Nanowires*, Advanced Materials, 12, 298-301.

[11]. Wu Y., Yang P. (2000) *Germanium Nanowire Growth via Simple Vapor Transport*, Chemistry of Materials., 12, 605-607.

[12] Elouali S., Bloor L. G., Binions R., Parkin I. P., Carmalt C. J., Darr J. A. (2011) *Gas Sensing with Nano-Indium Oxides (In_2O_3) Prepared via Continuous Hydrothermal Flow Synthesis*, Langmuir 2012, 28, 1879−1885.

[13] Zhang Z., Goodall J. B. M., Brown S., Karlsson L., Clark R. J. H., Hutchison J. L., Rehmanb I. U. Darr J. A. (2009) *Continuous hydrothermal synthesis of extensive 2D sodium titanate ($Na_2Ti_3O_7$) nano-sheets*, Dalton Transactions, 2010, 39, 711–714.

[14] Heath J. R., LeGoues F. K. (1993) *A liquid solution synthesis of single crystal germanium quantum wires*, Chemical Physics Letters, Elsevier, 208, 263-268.

[15] Wang X., Li Y. (2001) *Selected-Control Hydrothermal Synthesis of α- and β-MnO_2 Single Crystal Nanowires*, Journal of the American Chemical Society, 124, 2880-2881.

[16] Sharma M., Kuanr B. K. (2015) *Electrodeposition of Ferromagnetic Nanostructures*, Electroplating of Nanostructures (Ed. Aliofkhazraei M.), InTech, Chapter 3, 49-73, ISBN 978-953-51-2213-5.

[17] Plowman B. J., Bhargava S. K., O'Mullane A. P. (2011) *Electrochemical fabrication of metallic nanostructured electrodes for electroanalytical applications*, Analyst, 136, 5109-5119.

[18] L. Silipigni, F. Barreca, E. Fazio, F. Neri, T. Spanò, S. Piazza, C. Sunseri, R. Inguanta (2014) *Template Electrochemical Growth and Properties of Mo Oxide Nanostructures*, Journal of Physical Chemistry C, 118, 22299-22308.

[19] R. Inguanta, S. Piazza, C. Sunseri (2008) *Influence of electrodeposition techniques on Ni nanostructures*, Electrochimica Acta, 53, 5766-5773.

[20] F. Cerrina, C. Marrian (1996) *A Path to Nanolithography*, Materials Research Society, 21, 56-62.

[21] Zhao X. M., Xia Y., Whitesides G. M: (1997) *Soft lithographic methods for nano-fabrication*, Journal of Materials Chemistry, 7(7), 1069–1074.

[22] Gibson J. M. (1997) *Reading and Writing with Electron Beams*, Physics Today, October, 56-61.

[23] Matsui S., Ochiai Y. (1996) Focused ion beam applications to solid state devices, Nanotechnology, 7, 247-258.

[24] Hong S., Zhu J., Mirkin C. A. (1999) *Multiple Ink Nanolithography: Toward a Multiple-Pen Nano-Plotter*, Science, 286, 523-525.

[25] Levenson M. D. (1995) *Extending optical lithography to the gigabit era*, Solid State Technology, 38, 57-66.

[26] Dunn P. N. (1994) *X-ray's future. A Cloudy Picture*, Solid State Technology, 37, 49-68.

[27] Wang Y., Angelatos A. S., Caruso F. (2007) *Template Synthesis of Nanostructured Materials via Layer-by-Layer Assembly*, Chemistry of Materials, 20, 848-858.

[28] Cocchiara C., Inguanta R., Piazza S., Sunseri C., (2016) *Nanostructured Anode Material for Li-ion Battery Obtained by Galvanic Process*, Chemical Engineering Transactions, 47, 73-78.

[29] Schonenberger C., van der Zande B. M. I., Fokkink L. G. J., Henny M., Schmid C., Kru1ger M., Bachtold A., Huber R., Birk H., Staufer U. (1997) *Template Synthesis of Nanowires in Porous Polycarbonate Membranes: Electrochemistry and Morphology*, Journal of Physical Chemistry B, 101, 5497-5505.

[30] Patella B., Inguanta R., Piazza S., Sunseri C. (2016) *Nanowire Ordered Arrays for Electrochemical Sensing of H_2O_2*, Chemical Engineering Transactions, 47, 19-24.

[31] Sunseri C., Cocchiara C., Ganci F., Moncada A., Oliveri R. L., Patella B., Piazza S., Inguanta R. (2016) *Nanostructured Electrochemical Devices for Sensing, Energy Conversion and Storage*, Chemical Engineering Transactions, 47, 43-48.

[32] Inguanta R., Spanò T., Piazza S., Sunseri C., Barreca F., Fazio E., Neri F., Silipigni L. (2015) *Electrodeposition and characterization of Mo oxide nanostructures*, Chemical Engineering Transactions, 43, 685-690.

[33] Moncada A., Piazza S., Sunseri C., Inguanta R. (2015) *Recent Improvements in PbO_2 Nanowire Electrodes for Lead-Acid Battery*, Journal of Power Sources, 275C, 181-188.

[34] Battaglia M., Piazza S., Sunseri C., Inguanta R. (2014) *CuZnSnSe nanotubes and nanowires by template electrosynthesis*, Advanced Science and Technology, 93, 241-246.

[35] Patella B., Inguanta R., Piazza S., Sunseri C. (2017) *A Nanstructured Sensor of Hydrogen Peroxide*, Sensors and Actuators B 245, 44-54.

[36] Ganci F., Inguanta R., Piazza S., Sunseri C., Lombardo S. (2017) *Fabrication and Characterization of Nanostructured Ni and Pd Electrodes for Hydrogen Evolution Reaction (HER) in Water-Alkaline Electrolyzer*, Chemical Engineering Transactions, 57, 1591-1596.

[37] Paunovic M., Schlesinger M. (2006) *Fundamental of Electrochemical Deposition, Second Edition*, John Wiley & Sons, Inc.

[38] Pourbaix M. (1974) Atlas of Electrochemical Equilibria in Aqueous Solutions, National Association of Corrosion Engineers.

[39] Battaglia M., Inguanta R., Piazza S., Sunseri C. (2014) *Fabrication and characterization of nanostructured Ni–IrO2 electrodes for water electrolysis*, International Journal of Hydrogen Energy, 39, 16797-16805.

6. Nanostructures Morphological and Chemical Characterization

After nanostructure fabrication and membrane dissolution, each electrode was morphologically and chemically characterized in order to verify the electrode uniformity, the shape of the nanostructures, and the complete dissolution of the polycarbonate membrane.

Morphology was investigated using a FEG-ESEM microscope (model: QUANTA 200 by FEI), equipped with Energy Disperse Spectroscopy (EDS) probe. The crystallographic structure was investigated by a RIGAKU X-ray diffractometer (model: D-MAX 25600 HK). Diffraction patterns were obtained in the 2θ range from 10° to 100° with a sampling width of 0.01° and a scan speed of 0.5 step/sec, using Ni-filtered Cu Kα radiation (λ= 1.54 Å). The tube voltage and current were set at 40 kV and 40 mA, respectively. Diffraction peaks were identified by comparison with ICDD database [1].

6.1. Ni NWs Morphological and Chemical Characterization

Figs. 6.1-6.2 show the typical morphology of Ni NWs at two different magnifications. Ni-NWs had a cylindrical regular shape almost 250 nm diameter and 9-10 μm long (Figure 6.3). The high level of interconnection is due to the morphology of the template, which was completely removed after dipping in dichloromethane.

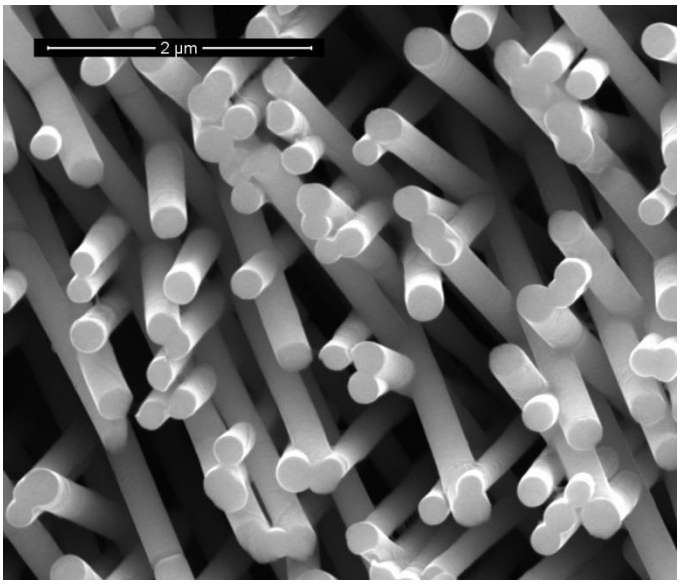

Figure 6.1 – SEM image of Ni NWs at high magnification

The chemical composition and crystallographic structure were determined through EDS and XRD analyses, respectively. Fig. 6.4 shows that Ni NWs are pure Ni. In addition, the absence of both C and O peaks indicates the complete dissolution of the membrane. A typical XRD pattern of Ni NWs is shown in Fig. 6.5, where all peaks are attributable to Ni phases (card 4-850 of the ICDD database [1]) except for one very

weak peak likely due gold (card 4-784), coming from the film initially sputtered on one side of the membrane in order to make it electrically conductive.

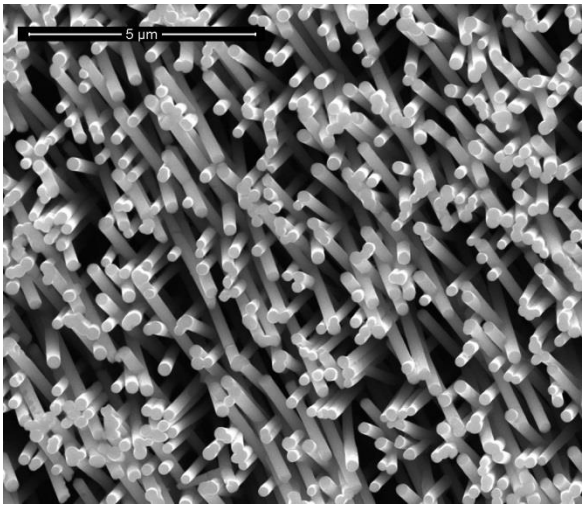

Figure 6.2 – SEM image of Ni NWs at intermediate magnification

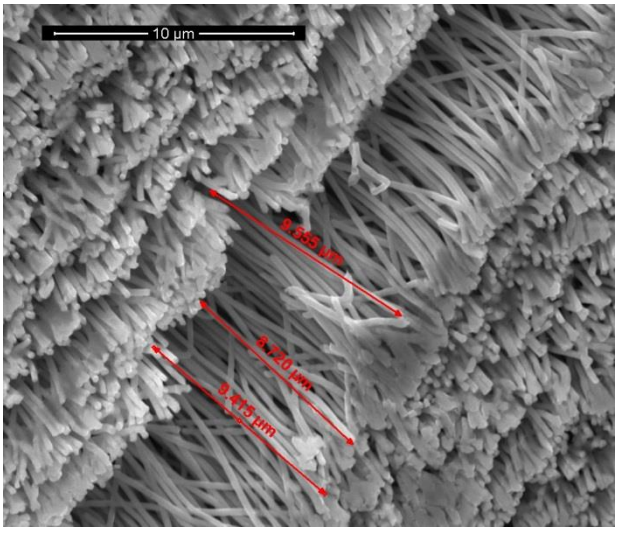

Figure 6.3 – Typical Ni NW length.

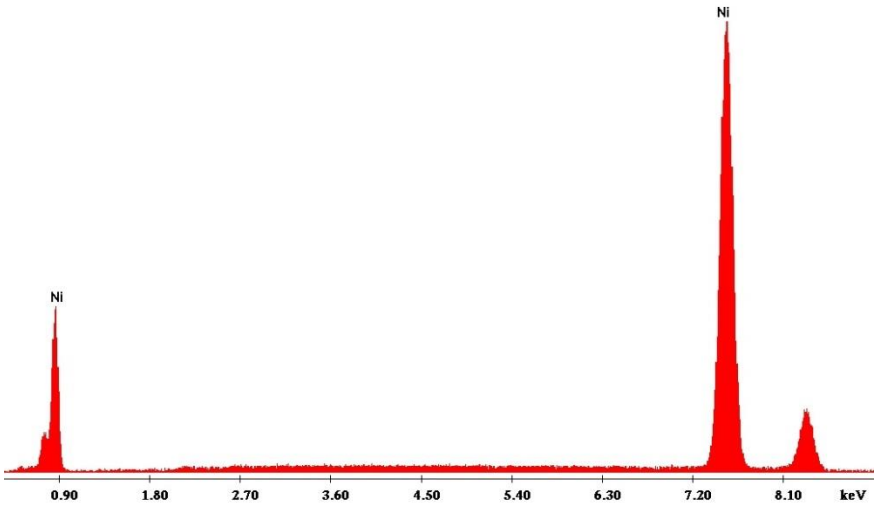

Figure 6.4 – Typical EDS spectrum of Ni NWs.

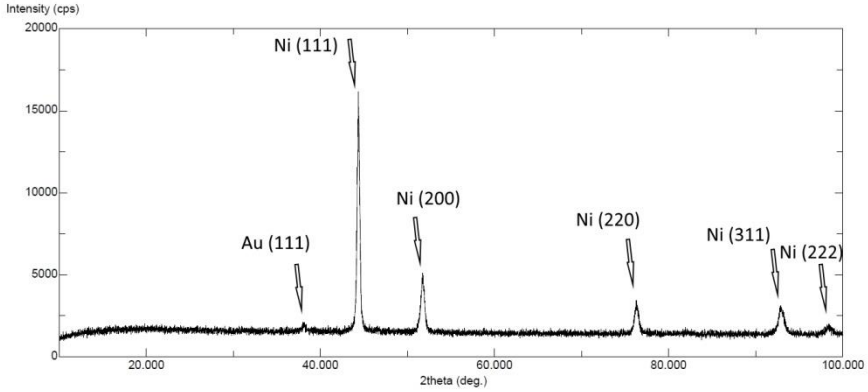

Figure 6.5 – Typical XRD pattern of Ni NWs.

6.2. Morphological and Chemical Characterization of Ni NWs functionalized with Pd particles

Pd nanoparticles were deposited on Ni NWs surface after template dissolution. The surface concentration of Pd NWs was increasing with deposition time as shown in Figs. 6.6-6.8 where morphologies of the functionalized Ni NWs are shown after 1, 5, and 10 min. of deposition.

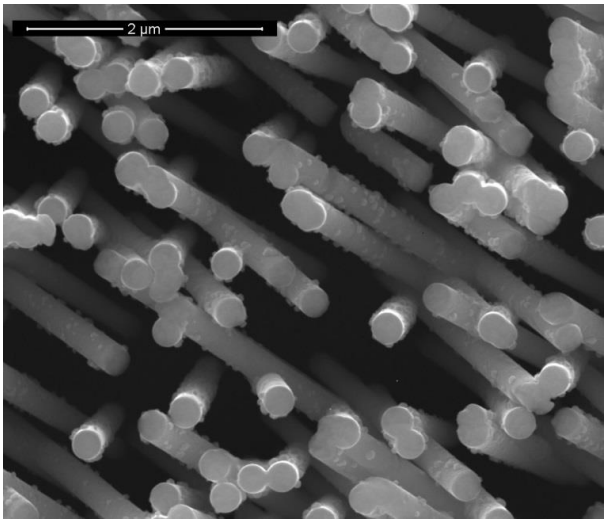

Figure 6.6 – SEM image of Ni NWs after of 1 min long deposition of Pd nanoparticles

Instead, Figs. 6.9-6.10 show typical detailed morphology of Ni NWs functionalized through deposition of Pd nanoparticles. In particular, Fig. 6.11 shows that the Pd nanoparticles present a regular spherical shape with a diameter between 60 and 70 nm.

In addition, the EDS spectrum of Fig. 6.11 shows the presence of Ni peaks, due to NWs and current collector, and Pd peaks, due to nanoparticles.

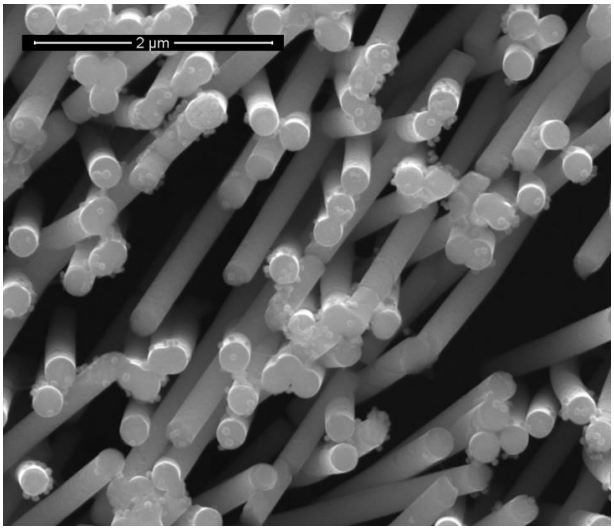

Figure 6.7 – SEM image of Ni NWs after of 5 min long deposition of Pd nanoparticles

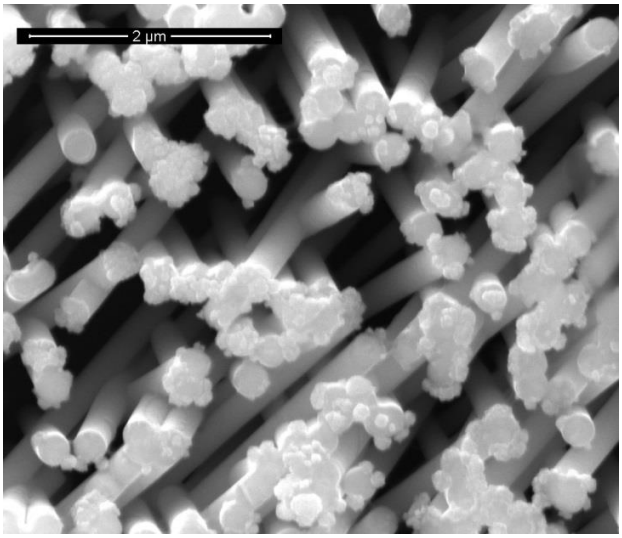

Figure 6.8 – SEM image of Ni NWs after of 10 min long deposition of Pd nanoparticles

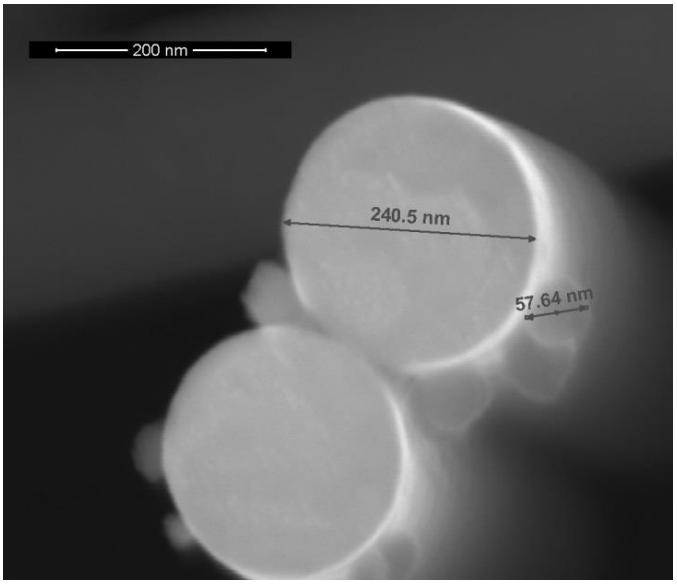

Figure 6.9 – Details of the NWs and Pd nanoparticle size after 5 min long deposition of Pd

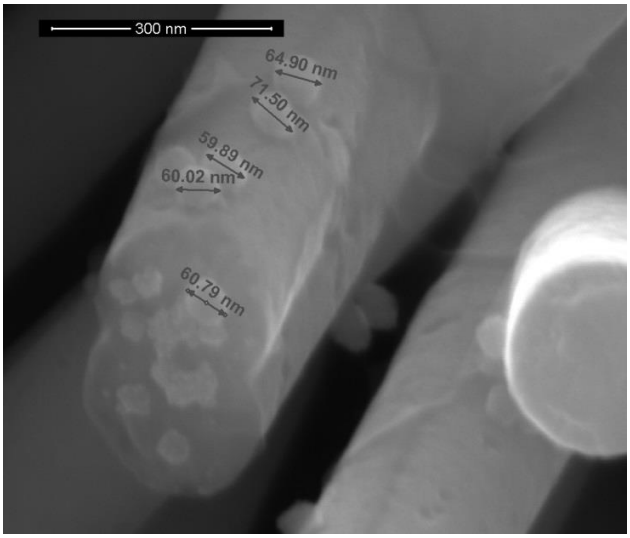

Figure 6.10 – Details of the Pd nanoparticle distribution on Ni NWs after 5 min long deposition of Pd

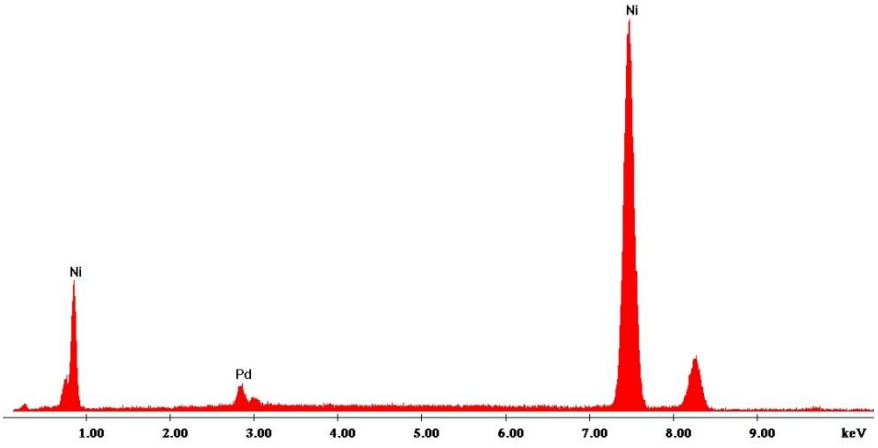

Figure 6.11 – Typical EDS spectrum of Ni NWs functionalized with Pd nanoparticles

6.3. Pd NWs Morphological and Chemical Characterization

Fig. 6.12 shows the Pd NWs morphology, which is similar to that one of Ni NWs, except for the surface roughness, which can be attributed to both different nature of the deposit and fabrication method. Fig. 6.13 shows EDS spectrum where peaks of Pd, Ni, and Au are present. The presence of gold is due to the film initially sputtered on one side of the template to make it conductive, while Ni peak is due to the layer acting as a current collector, which was deposited on the sputtered film. It was chosen to deposit Pd NWs on a Ni current collector in order to compare two chemically different nanostructures in otherwise identical conditions. By this way, it has been possible to compare each nanostructured deposit and relate the differences only to the chemical nature of the NWs.

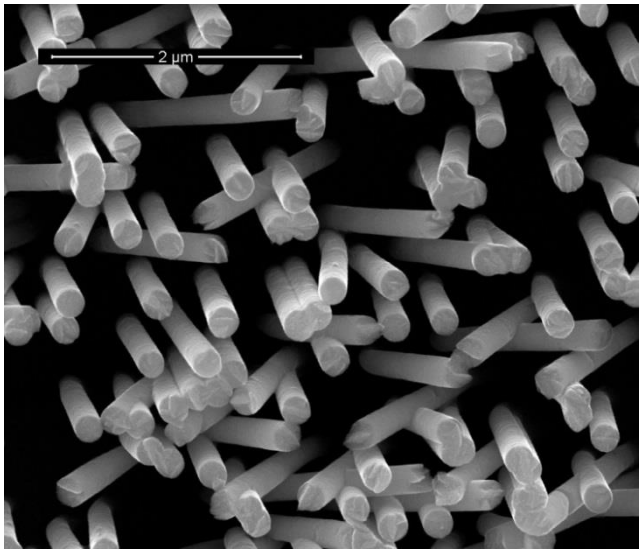

Figure 6.12 – SEM image of Pd NWs

Fig. 6.14 shows a typical XRD pattern of Pd NWs (card #87–367 of the ICDD database [1]), where also Ni peaks are present, likely in EDS spectrum. Fig. 6.14 shows the presence of one peak which cannot be attributed to either Pd or Ni. According to EDS spectrum of Fig. 6.13 and card #4-784 of ICDD database, this weak peak was attributed to gold likely due to the sputtered film.

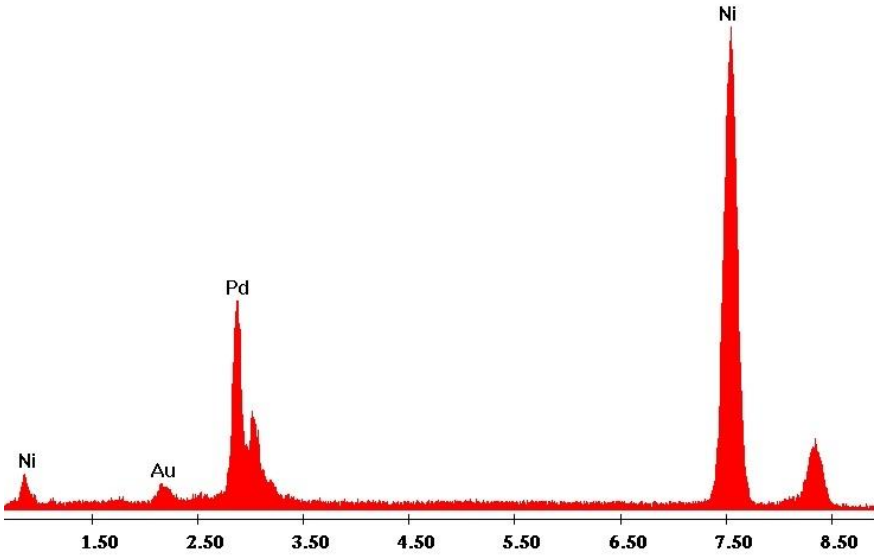

Figure 6.13 – EDS spectrum of Pd NWs

.

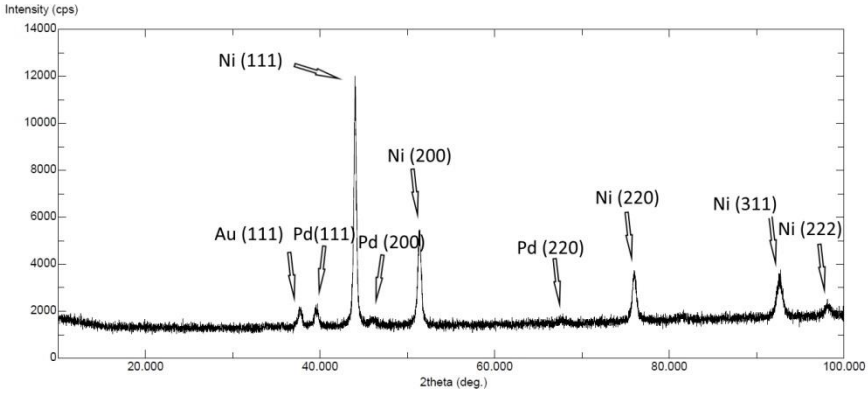

Figure 6.14 – XRD pattern of Pd NWs.

References

[1] International Centre for Diffraction Data, Power Diffraction File (2007), Pennsylvania USA, card number: Ni 4–850; Au 4–784; Pd 87–367.

7. Nanostructures Electrochemical Characterization

Electrochemical characterization was performed using a Cell Test System (Solartron, Mod. 1470 E, 8 channels). Data were recorded by a desk computer via MultiStat Software (Mod. UBS147010ES). All the characterization tests were performed in 30% w/w KOH aqueous solution. The water used for the solution was a deionized Millipore 18.2 MΩ cm resistivity. A Ni strip with a high surface area (> 20 cm^2) and an Hg/HgO (20 % KOH) electrode were employed respectively as counter and reference electrode.

7.1. Cyclic Voltammetry Characterization

The electrochemical characterization was performed by cyclic voltammetry (CV) conducted at 0.020 Vs^{-1} in the potential interval between 0.1 and -1.1 V vs. Hg/HgO. Fig. 7.1 shows the initial six cycles of a Ni strip. An anodic wave can be observed at about -0.45 V due to the oxidation of Ni to Ni^{2+} while the cathodic current is associated to the reaction

$$2H^+ + 2e^- = H_2 \qquad (7.1)$$

Whose Electrochemical Standard Potential is E° = -0.924 vs. Hg/HgO at pH = 14. The maximum cathodic current density at -1.1 V is a few higher than $-7*10^{-5}$ Acm^{-2}, while the maximum anodic current density is about 10^{-5} Acm^{-2} at 0.1 V. Ni NWs in the same conditions like Ni strip show a significant increase of the current density.

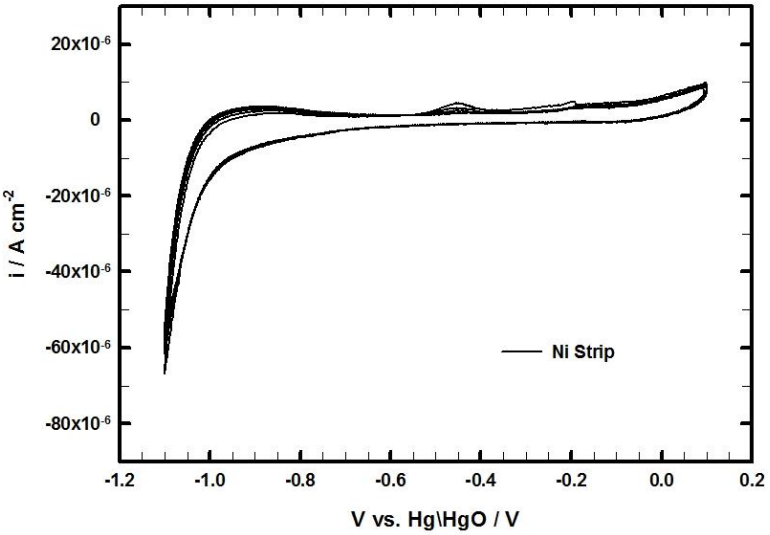

Figure 7.1 – Cyclic voltammetry of Ni strip in 30 % KOH at room temperature (scan rate 0.020 Vs^{-1}).

Fig. 7.2 shows a cathodic current of $-5*10^{-3}$ Acm^{-2} at -1.1 V. Since the nature of the electrode of Fig. 7.2 is identical to that one of Fig. 7.1, we can exclude any electrocatalytic difference between the two electrodes, and to attribute the difference in current density to the increase of the real electrode area. This means that the real Ni NWs surface area is two orders of magnitude higher than the geometrical one. This finding is confirmed by comparing the anodic current at 0.1 V in the two cases as shown in Figs. 7.1-7.2.

Fig. 7.3 shows the electrochemical behavior of Ni NWs + Pd nanoparticles when subjected to CV in identical conditions of Ni strip and NWs. The Pd deposition time chosen for the electrochemical characterization was 5 min. For this electrode, the CV response was similar to Ni NWs one (Fig. 7.2). The only difference was the presence of

an anodic peak at -0.85 V. This peak can be attributed to hydrogen oxidation according to J.M. Skowronski et. Al. [1].

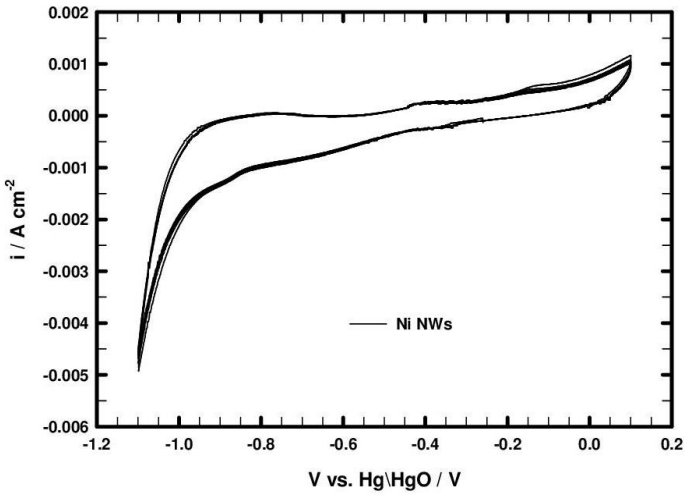

Figure 7.2 – Cyclic voltammetry of Ni NWs in 30 % KOH at room temperature (scan rate 0.020 Vs^{-1}).

The same peak had been observed in Fig. 7.4 in the Pd NWs CV. The potential scanning started from about -0.274 V vs. Hg/HgO toward cathodic direction up to -1.1 V where hydrogen evolution occurred. On the reverse scan, a very pronounced anodic peak can be observed at - 0.75 V vs. Hg/HgO whose intensity was decreasing with cycling. Also the maximum cathodic current density at -1.1 V was decreasing under cycling. This behavior can be attributed to the specific interaction between Pd and hydrogen. Palladium metal behaves as an hydrogen sponge because it is able to intercalate great amount of it, so that is used for syngas filtering as described by Yun S. and Oyama S.T. in their

valuable review [2]. During, the first cycle, when Pd NWs were fresh, the maximum amount of hydrogen was intercalated into Pd, with consequent very high anodic c.d. peak at -0.75V vs Hg/HgO where oxidation of the absorbed hydrogen likely occurred. Then, the anodic peak intensity progressively diminished because the amount of intercalated hydrogen was decreasing under cycling.

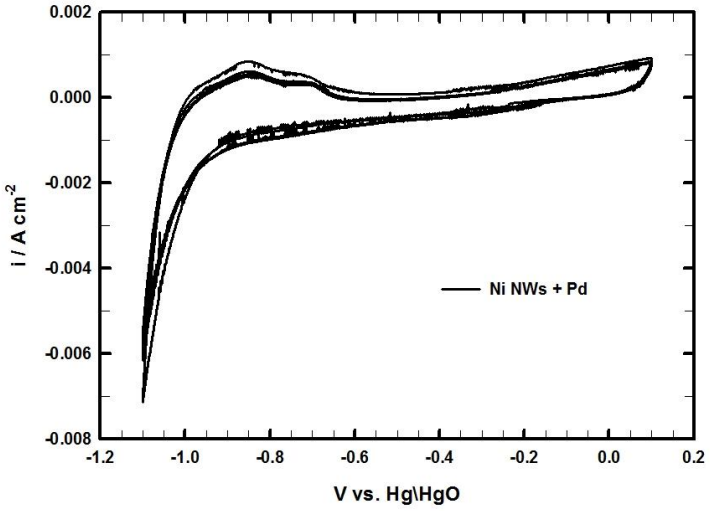

Figure 7.3 – Cyclic voltammetry of Ni NWs + Pd nanoparticles in 30 % KOH at room temperature (scan rate 0.020 Vs^{-1})

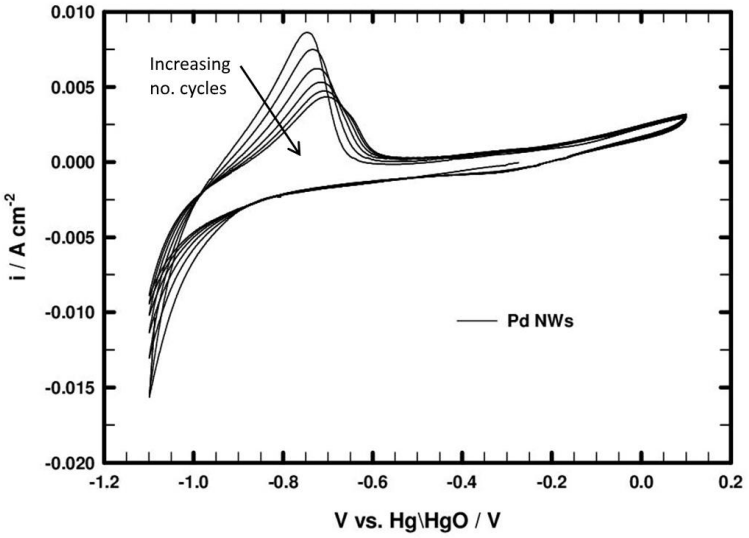

Figure 7.4 – Cyclic voltammetry of Pd NWs in 30 % KOH at room temperature (scan rate 0.020 Vs^{-1})

7.2. Quasi-Steady State Polarization Characterization

Fig. 7.5 compares the electrocatalytic behavior for Hydrogen Evolution Reaction (HER) for different types of electrodes, and evidences that the overpotential is significantly lower for the nanostructured ones. Quasi-steady state polarizations were carried out by means of a potential sweep from the thermodynamic value of hydrogen evolution (0 V vs. RHE) to -2 V vs RHE, scan rate 0.1667 mVs^{-1}. The potential values are iR-corrected. By comparing the Ni NWs with and without Pd nanoparticles, the nanoparticles presence seems to improve performance at low

overpotential. However, this improvement disappears at higher current density, making the performance identical for both electrodes.

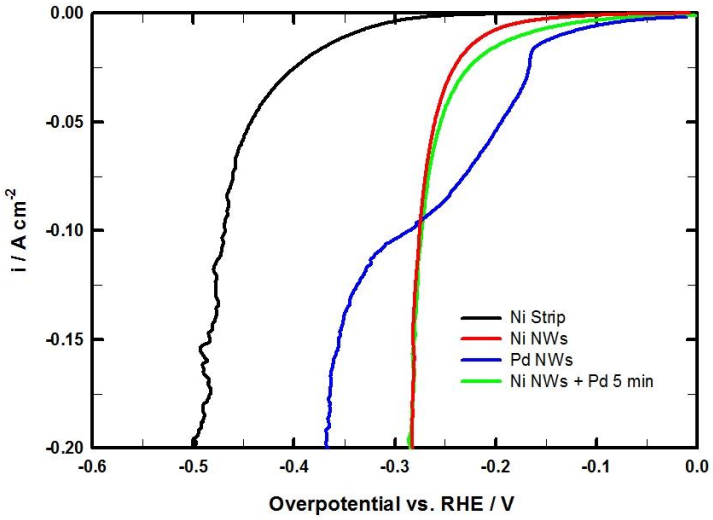

Figure 7.5 – Quasi-steady state polarization curves for Ni strip, Ni NWs, Ni NWs + Pd 5 min and Pd NWs in 30 % w/w KOH solution at room temperature. Overpotential referred to hydrogen scale at pH 14 (RHE)

In the comparison between Pd and Ni nanostructured electrodes, Fig. 7.5 also shows that hydrogen evolution is kinetically favored on Pd NWs up to a cathodic current density a few higher than 0.10 Acm^{-2}. Then, hydrogen evolution occurs at lower overpotential on Ni NWs. This behavior can also be explained by the nature of palladium to form hydrides and to adsorb hydrogen. Once saturated, palladium no longer maintains the same electrocatalytic properties. This effect will be even more evident with the other characterizations.

7.3. Constant Current (Galvanostatic) Characterization

Constant current density tests on Ni and Pd nanostructures electrodes for short time of working were also conducted. Fig. 7.6 confirms that Ni NWs cathode polarized at 0.5 Acm^{-2} better works than Pd NWs one in otherwise identical conditions. In any case, both electrodes decay under working at about the identical rate. For regenerating, they were held at open circuit for half an hour, and then were polarized again at the same current density of 0.5 Acm^{-2}, and the dashed lines were recorded.

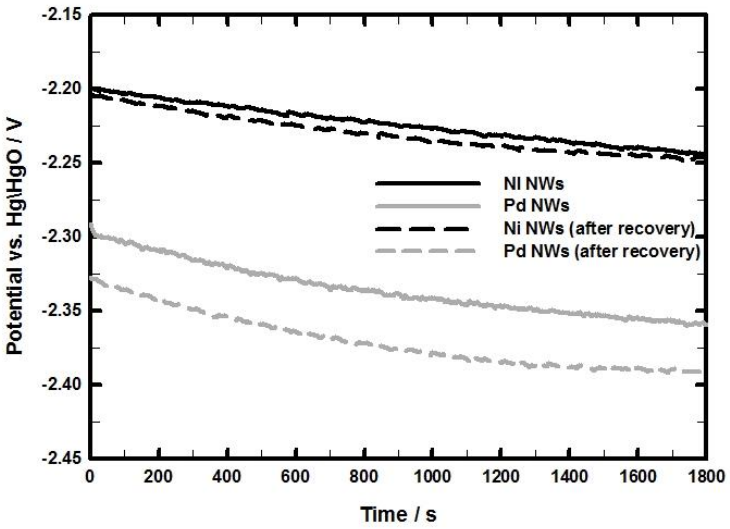

Figure 7.6 – Potential vs time plots for hydrogen evolution in 30% KOH at room temperature and current density of 0.5 Acm-^{2}. Solid lines: short time stability of fresh Ni and Pd NWs. Dashed line: after 0.5 hrs. at open circuit.

Fig. 7.6 clearly shows that the regeneration is practically complete in the case of Ni NWs, while is partial in the case of Pd NWs, because, likely, some adsorbed hydrogen remains trapped inside palladium.

7.4. Ni NW Characterization

Based on the previously results, the best performance for the HER was obtained with the Ni NW electrode. Thus, further characterizations have been conducted on this electrode. The plot of Fig. 7.7 shows a logarithmic dependence of the overpotential on the current density in the range from about $2.8*10^{-2}$ to 10^{-1} Acm^{-2} for Ni NWs cathode in 30% KOH.

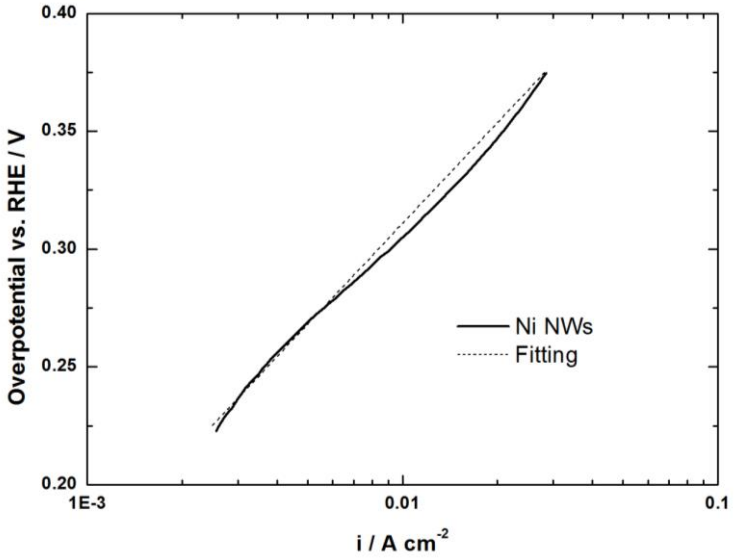

Figure 7.7 – Linearity range of the HER overpotential on logarithmic current density for Ni NWs

Assuming unitary current efficiency for hydrogen evolution, the linear dependence gives the contribution of the reaction overvoltage to the total one, which in our case is due only to ohmic drop and reaction overvoltage. The third contribution, concentration overvoltage, can be neglected because water concentration, which is the source of hydrogen in alkaline solution, is practically constant. The slope of the line of Fig. 7.7 is 142 mV/decade. Fig. 7.8 shows the Ni NWs cathode overpotential vs. current density as an experimentally measured (curve a), and the reaction overvoltage vs. current density obtained by the slope of the Fig. 7.7 line. At 0.5 Acm^{-2}, which is the lowest current density of technological interest, the reaction overvoltage accounts for about 40% of the total overvoltage.

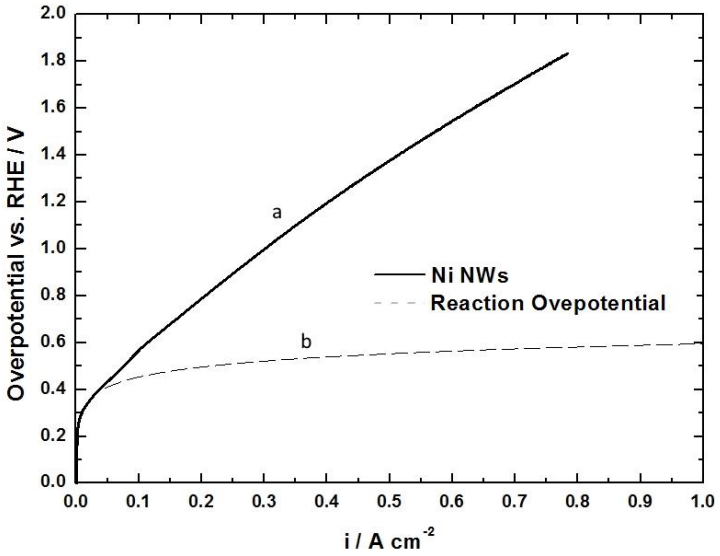

Figure 7.8 – Overpotential vs. current density for Ni NWs in 30% KOH at room temperature: (a) experimental curve, (b) reaction overvoltage from Fig. 7.7

The lowest operative current density is considered 0.5 Acm^{-2}, because at this current density, a nominal hydrogen production rate of 186.53 ghr^{-1} is achieved for an electrode surface of 1 m^2, and unitary current efficiency. The importance of the result of Fig. 7.8 is in showing that the prevalent dissipative contribution for electrochemical hydrogen production from alkaline solutions is due to the ohmic drop. This finding is highly encouraging because the ohmic drop can be adjusted through a good engineering of the cell, therefore, it can be diminished through a suitable cell design. Ni NW electrode was also tested as a cathode for 60 hrs. without interruption at 0.5 Acm^{-2} and room temperature.

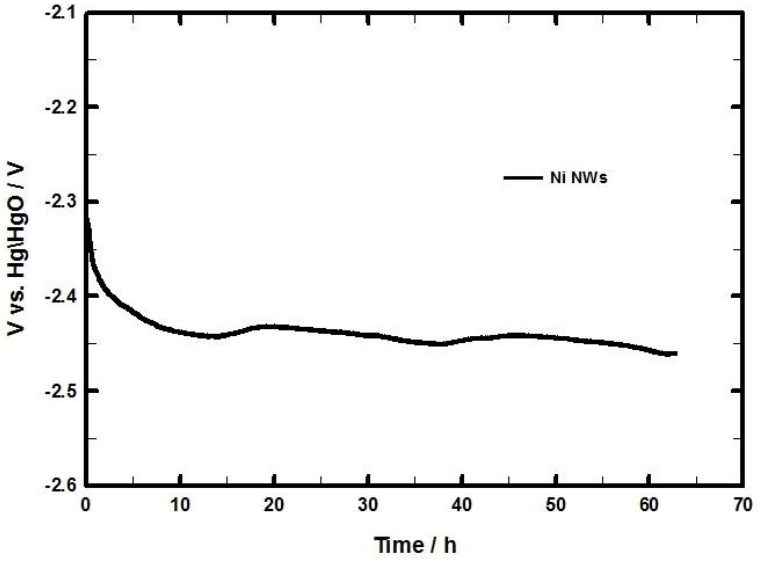

Figure 7.9 – Long time stability of fresh Ni NWs in 30 % w/w KOH solution at 0.5 Acm^{-2}

Fig. 7.9 shows that the potential reaches a steady state value around -2.45 V vs. Hg/HgO, with a decay of 0.15 V from the initial value that was a few more negative than -2.3 V. Taking into account that most

of such a decay occurs within the first 10 hrs. (0.14 V), the result after 60 hrs. appears as satisfying in terms of electrode stability.

In light of these results, an electrolytic cell with both Ni NWs electrodes was designed and then realized and tested. The cell design schemes and the obtained results are presented in chapter 8.

References

[1] Skowroński, J.M., Czerwiński, A., Rozmanowski, T., Rogulski, Z., Krawczyk, P. (2007) *The study of hydrogen electrosorption in layered nickel foam/palladium/carbon nanofibers composite electrodes*, Electrochimica Acta, 52 (18), 5677-5684

[2] Yun S. and Oyama S.T. (2001) *Correlations in palladium membranes for hydrogen separation: A review*, Journal of Membrane Science, 375 (1-2), 28-45.

8. Cell Design and Tests

Once electrochemical tests were performed on electrodes in terms of performance and stability, a cell was first conceived, designed and then realized to test a real operation. Fig. 8.1 shows the cell design with all the compacted parts. Fig. 8.2 represents a half-cell exploded view. The red parts are the two electrodes, anode and cathode. The diaphragm is shown in yellow. In green, gasket sheets are represented.

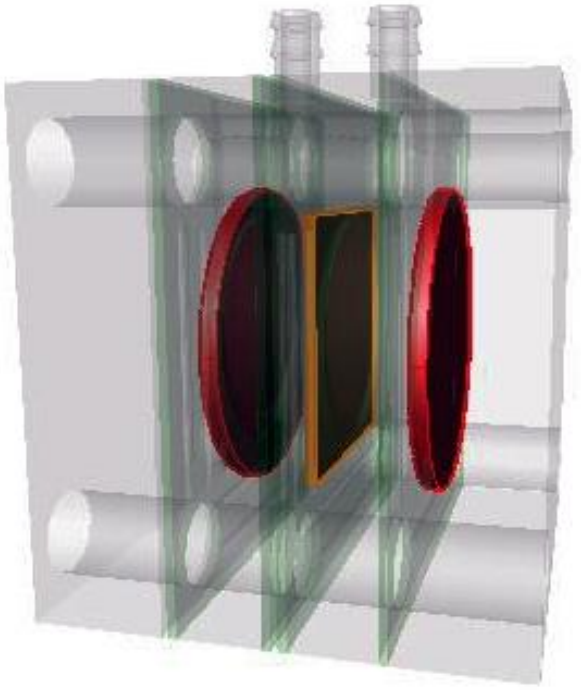

Figure 8.1 – Compacted cell design.

The internal blocks have two cylindrical holes, with horizontal axis and vertical axis. The first one is intended for containing the

electrolyte, while the second one is used to put in the electrolyte once the cell is mounted, and to allow the gas exit. The external blocks have a recess adapted to contain an external electrical connection for the electrodes. Gasket sheets, internal and external blocks have four horizontal cylindrical holes on the four corners to allow the passage of bolts that hold the cell parts together. On the lateral blocks surfaces, reliefs are present to allow a better seal of the gasket.

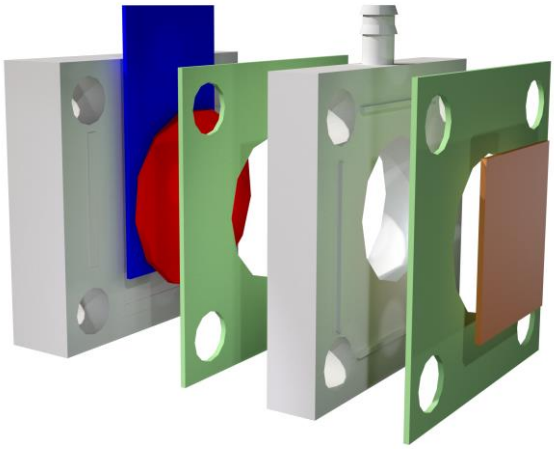

Figure 8.2 – Exploded view of half-cell design.

Starting from this cell design, the real cell was built. The central and external blocks were fabricated with a Zortrax M200 3D printer [1]. The material used for manufacturing was Acrylonitrile Butadiene Styrene (ABS). The dimensions of the blocks were 60x60x10 mm. The central hole diameter was 25 mm which corresponds to a surface of about 5 cm^2. The gasket sheets were made by 2 mm thick Ethylene-Propylene Diene Monomer (EPDM) rubber. The diaphragm was 35 µm thick polypropylene.

The cell with the characteristics listed above was tested with two pairs of electrodes, namely Ni strip and Ni NWs. Once the cell was closed, the distance between cathode and anode was about 25 mm. Also for these tests, the electrolyte used was 30% w/w KOH aqueous solution. Quasi-steady state polarizations were carried out by means of a cell potential sweep from the cell potential thermodynamic value E° (Eq. 3.8) to 4.5 V, scan rate 0.1667 mVs^{-1}. The tests were interrupted once a current density of 0.5 Acm^{-2} was reached.

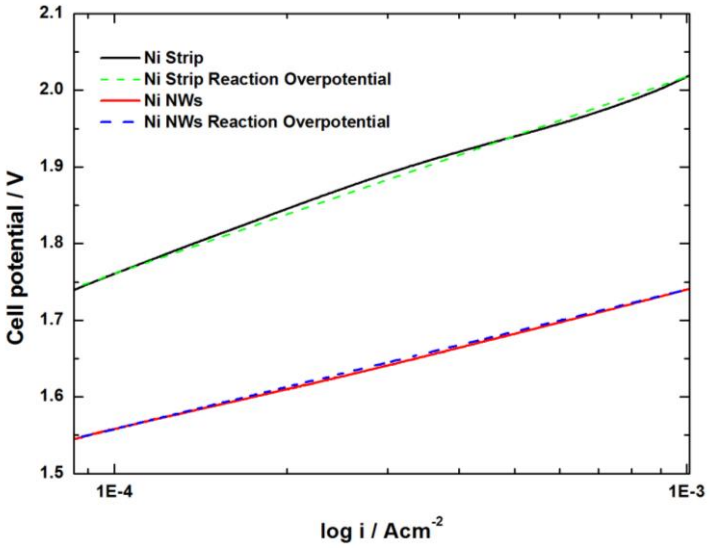

Figure 8.3 – Linearity range of the cell potential vs. logarithmic current density for Ni Strip and Ni NWs. Solid lines: experimental curves; dashed lines: fitted curves.

Fig. 8.3 shows the interval throughout which the cell potential is linear with respect to a logarithmic current density. The line slopes had been extrapolated through the best matching of the experimental curves

trends in the current range between 10^{-3} and 10^{-4} Acm^{-2}. The slopes values were 0.257 V/decade for Ni strip and 0.182 V/decade for Ni NWs. This result indicates how the nanostructures lowered reaction overvoltage. In addition, the improvement increases with current densities. The solid lines of Fig. 8.4 show the cell potential vs current density for Ni Strip and for Ni NWs, while the dashed lines show reaction overvoltage vs. current density obtained by the slopes of Fig. 8.3.

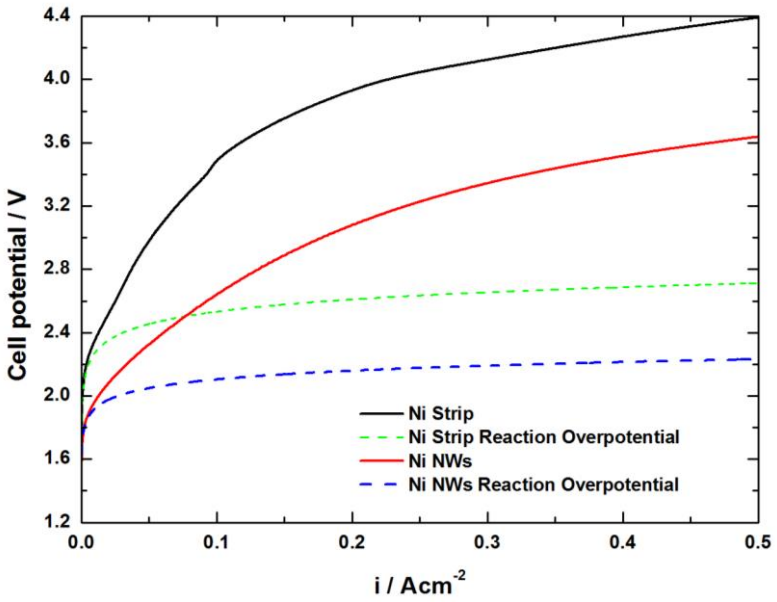

Figure 8.4 – Cell potential vs. current density for Ni Strip and Ni NWs. Solid lines: experimental curves; dashed lines: reaction overpotential from Fig. 8.3.

At 0.5 Acm^{-2}, the cell potential for Ni NWs and Ni Strips was 3.62 V and 4.4 V respectively. Using the Eq. 3.13, the cell efficiency was 40.9% and 33.6% respectively. Therefore under these conditions, the

nanostructured electrodes improved the cell efficiency by 7.3%. Furthermore, taking 3.62 V as reference, the current density of the Ni Strip is about 0.1 Acm^{-2}, five times lower than that of Ni NWs. This means that with nanostructures it would be possible to produce 5 times more hydrogen and oxygen at the same efficiency. Really, this result was far lower than the expected one according with surface gain passing from flat to nanostructured surface.

In any case, the results presented in this chapter and in the previous ones, show how the nanostructures significantly improve the cell performances. However, major improvements are necessary to achieve competitive cell efficiency levels. Firstly, an improvement in electrocatalysis of the electrodes is possible. Tests are in progress on the fabrication and characterization of nanostructured electrodes with Ni-Co alloys for improving the electrocatalysis features. Secondly, a further development of cell design is already underway. The thickness reduction of internal blocks would lead to the reduction of the distance between the electrodes and to a consequent reduction of the ohmic yields. Moreover, in the future it is planned to make the cell work with a continuous recycling of the electrolyte. This would favor the outflow of gas and avoid the electrolyte concentration variation over time. Another important parameter to take into consideration is the temperature. In fact, all the tests previously reported were carried out at ambient temperature. The overvoltages could be greatly reduced, especially at high current densities, if electrolysis is conducted at higher temperature than the room one. Finally, a study on the wettability of nanostructures is necessary to ensure that the entire surface operates.

References

[1] Zortrax: https://zortrax.com/printers/zortrax-m200/

9. Conclusions

In this work, it has been successfully investigated the use of nanostructured materials as electrodes for hydrogen production through alkaline solution water splitting. The results are highly encouraging because it has been found an immediate benefit in the high ratio of true surface area to geometrical one, which is about 70. In addition, it has been found that the major future improvements may come from the electrochemical cell design, which must be complying with the electrode morphology.

The focus was on the fabrication of the nanostructured electrodes. For the sake of simplicity, Nickel was chosen as an electrode material because extensively used in the current technology of hydrogen production from aqueous alkaline solutions. Nickel was deposited in the form of NWs inside the pores of a polycarbonate membrane, acting as a template, which was easily removed at the end of the deposition by chemical etching in an organic compound guaranteeing fast and complete dissolution. Prior to growing the Nickel nanostructures a layer of the same metal, acting as a current collector, was deposited on the gold film, which was initially deposited on one side of the template for making it electrically conductive. The growth of the nanostructures was conducted through a procedure developed some years ago in the same Lab where the present work was conducted. Despite this, several challenges have been faced in order to obtain dimensionally stable nanostructures to be used successfully as electrodes under gases evolution. A specific investigation was also conducted on deposition of the Nickel current collector in order to obtain a compact and dimensionally stable layer able to mechanically

sustain nanostructures. At this aim, Nickel layer was deposited at a potential of -1.25 V vs. SCE in order to limit the simultaneous hydrogen evolution otherwise leading to scarcely compact layer.

Similar challenges were faced for deposition of the nanostructures. In this case, a pulsed voltage was applied and compact NWs, firmly connected to the Nickel layer, were obtained. Despite the true surface of the nanostructures was found to be about 70 times greater than the geometrical one, the performance tests conducted in a properly designed electrochemical cell showed that the improvement is much more limited, because typically does not exceed 5 times. This significant reduction can be attributed to different causes. The most likely of these is the trapping of the evolving gases inside the nanostructures. In other words, a significant advantage in using nanostructured electrodes in place of strips is the very high real surface, as determined through voltammetric characterization. Unfortunately, much of the advantage was largely lost owing to the trapping of the gases produced. This drawback can be overcome through a proper hydrodynamic investigation of the fluid fluxes throughout the cell, which is already in progress. Other activities are continuing dealing with different electrocatalysts such as Ni-Co NWs and higher compact assembly of the anode/separator/cathode block; all aimed to reducing the cell voltage and improving energy efficiency. In this scenario, a fundamental role will be played by the temperature. Since the attention has been focused on the morphology of the electrodes, being of primarily importance to discover the performances of the nanostructured electrode grown through electrodeposition in template, the tests were conducted at room temperature and atmospheric pressure. It has already planned an increase of the temperature up to 60 – 80 °C,

while the role of the pressure will be exploited successively in dependence on specific applications.

Other significant results found in the present work are the faradaic efficiency, which reached the maximum value of 100% and the stability of the electrodes at 60 hrs. which is highly satisfying.